IMAGE

Grant Agreement Number 608553

IMAGE
## Integrated Methods for Advanced Geothermal Exploration
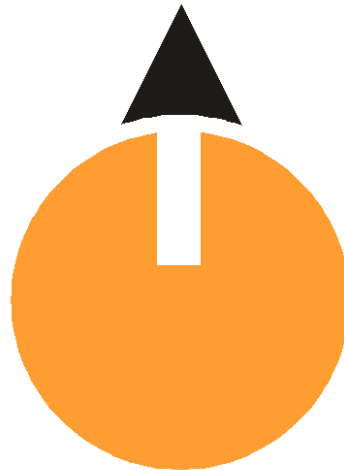
IMAGE-D7.04:
Resistivity techniques.
Electromagnetic Soundings in the Litomerice Geothermal Area (Czech Republic).

Responsible author	P. Wawrzyniak (BRGM)
Responsible WP-leader	Jan Hopman (TNO)
Contributions by:	P. Wawrzyniak (BRGM) M. Darnet (BRGM) N. Coppo (BRGM) J.F. Girard (BRGM)

Executive Summary

Within the frame of the FP7 European Project IMAGE, a special emphasis was put on improving and testing exploration techniques (WP7) in peri-urban environments, especially geophysical methods like seismic, gravimetry, magnetics and electromagnetics. In this report, we will focus on electromagnetic techniques for resistivity mapping.

Magnetotelluric (MT) method is widely used for exploration in geothermal areas. The challenge is that such a passive method is severely affected by electromagnetic (EM) noise induced by anthropogenic activities such as cities and industries. In particular, MT exploration is almost not feasible in countries where trains are powered by DC-current (such as in Czech Republic and some other regions in Europe). As an alternative, we proposed to deploy active source EM techniques (Controlled Source EM) using surface and borehole high power emission to improve the EM signal to noise ratios and allow mapping resistivity variations at the depth of the geothermal targets.

To demonstrate the feasibility of active and passive electromagnetic measurements for geothermal exploration, a geophysical survey has been performed in the area of Litoměřice (Czech Republic) where a geothermal exploration borehole (2 km deep) has been drilled in the Bohemian massif. Measurements have been performed from 6 to 11th September 2014 by BRGM and Geomedia staff, with the logistical help of Litoměřice city. The survey aims at measuring electrical resistivity variations at the depth of the alleged geothermal reservoir around ~2 km. For that purpose, a magnetotelluric (MT) profile has been performed at the same as a Controlled Source EM (CSEM) survey. To improve the MT signal quality, robust MT signal processing has been developed and applied using synchronous recordings performed locally (30 km) and at far (> 500 km) remote stations. To maximize the CSEM signal to noise ratio, a Long Electrode Mise-à-la-Masse (LEMAM) setup has been successfully deployed.

Analysis of the MT data shows that despite the use of a remote reference, MT data are corrupted at low frequency (<5Hz) by a permanent anthropic noise source. At higher frequencies, comparison with CSEM and borehole resistivity data shows that reliable resistivity measurements have been obtained. On the other hand, processing of the CSEM data shows the impact of industrial noise on CSEM data is minimal and only manifests itself at high frequencies (>32Hz). Modelling and inversion of such data shows that we can retrieve realistic resistivity measurements up to a depth of a few kilometers i.e. deep enough to image the geothermal reservoir of interest.

As a way forward in the next Work Package (WP8.2 application of exploration techniques) and as soon as the level of noise of an EM survey is believed to be an issue (e.g. due to the proximity of a city, train, high power line etc), we strongly recommend to compliment passive MT measurements with active CSEM measurements to image resistivity variations at reservoir depth. This can be done with single or double LEMAM setups but also with conventional surface only setups – a feasibility study is required to define on a case by case basis the appropriate approach.

Table of Content

1 Introduction

1.1 Background

Within the frame of the FP7 European Project IMAGE, a special emphasis was put on improving and testing exploration techniques (WP7) in peri-urban environments, especially geophysical methods like seismic, gravimetry, magnetics and electromagnetics. In this report, we will focus on electromagnetic techniques for resistivity mapping. Magneto-telluric (MT) method is widely used for exploration in geothermal areas. The challenge is that such a passive method is severely affected by electromagnetic (EM) noise induced by anthropogenic activities such as cities and industries. In particular, MT exploration is almost not feasible in countries where trains are powered by DC-current (such as in Czech Republic and some others regions in Europe). As an alternative, we propose to deploy active source EM techniques (Controlled- Source EM) using surface and borehole high power emission to improve the EM signal to noise ratios and allow mapping resistivity variations at the depth of the geothermal targets.

1.2 Objectives

As passive EM methods for geothermal exploration like MT are severely affected by electromagnetic (EM) noise induced by anthropogenic activities such as cities and industries, the first objective was to improve the signal quality of MT data acquired in urban areas like Litomerice area by applying robust MT signal processing using synchronous recordings performed locally and at far remote stations.
The second objective was to successfully acquire an active Controlled Source (CSEM) survey in the Litomerice area to complement the MT dataset and demonstrate that we can retrieve realistic resistivity measurements from CSEM measurements up to a depth of a few kilometers i.e. deep enough to image the geothermal reservoirs of interest.

1.3 Electromagnetic Survey

To address the aforementioned objectives, we performed an active and passive electromagnetic survey in the Litomerice area (Czech Republic). The MT survey consisted in 7 MT soundings along a profile and the CSEM survey was Long Electrode Mise-à-la-Masse (LEMAM) setup with a grid 25 recording sites spreading over a 4x4km area, two source polarizations and 6 transmitted frequencies.

1.4 Geological Background

During the past decade, the global trend of search for green energy resources has roused special interest in geothermal energy in Czech Republic. As a result, the first geothermal exploration borehole was drilled in Litoměřice in 2006 and Litoměřice has become the first site proposed for construction of a geothermal power plant or a heat plant in the Czech Republic.
The town of Litoměřice is located in the north-western part of the Bohemian Cretaceous Basin (BCB) near the intersection of two largest deep-seated fault zones in the region: the Eger Rift and Elbe Lineament, and lies in proximity of the Cenozoic volcanic centre of České středohoří (Capova, 2013). Other two major faults in the area are the Litochovice Fault (which is a part of the České středohoří Fault Zone) and the Litoměřice Fault. Most major faults are extensional and run in the E-W direction, normal faults of mostly Late Palaeozoic age running in the direction parallel to the Krušné hory Mts., i.e. SW-NE direction, are common as well. The Litoměřice Fault separates the

horst of the Opárno Crystalline Complex from the "Eger Rift", locally reaching the throw of up to 100 m. The basement of the area is formed of Proterozoic migmatites and orthogneisses belonging to the Krušné hory Crystalline Complex and of the so-called "Teplice rhyolite" or "Teplice porphyry" of Variscan age. The basement is overlain by the sequence of Permo-Carboniferous sediments of the four major formations of the Mšeno-Roudnice Basin (Kladno, Týnec, Slaný and Líně formations) with typical alternating mudstones and siltstones with sands and conglomerates and several coal-bearing horizons. The Permian formations are covered with Cretaceous sediments of the Eger part of the BCB, consisting of mudstones, marlstones and argillaceous limestones in the south with increasing proportion of sandstones towards the north. Sedimentation of the Upper Cretaceous is almost horizontal, with a slight inclination towards the north.

This area exhibits increased heat flow (locally exceeding 80 mW.m^{-2}). It is subject to discussion whether such heat flow should be attributed to post-volcanic activity of the area, to the deep-seated faults, a granitic pluton with intensive radiogenic heat production or a combination of these. The geological composition of the area is complicated as two major Variscan terranes – the Teplá-Barrandian and Saxothuringian – meet here. Further to the south-west, in the Karlovy Vary Region that is located within the so-called Eger Rift, naturally occurring thermal mineral waters are used in numerous spas and several hot springs and mud volcanoes are subject to protection as a national natural heritage. As this area is located on the same deep structure of Eger Rift, connection including some communication of thermal waters is possible. In the town of Děčín, which is only 30 km far from Litoměřice, thermal waters are used for district heating in a part of the town.
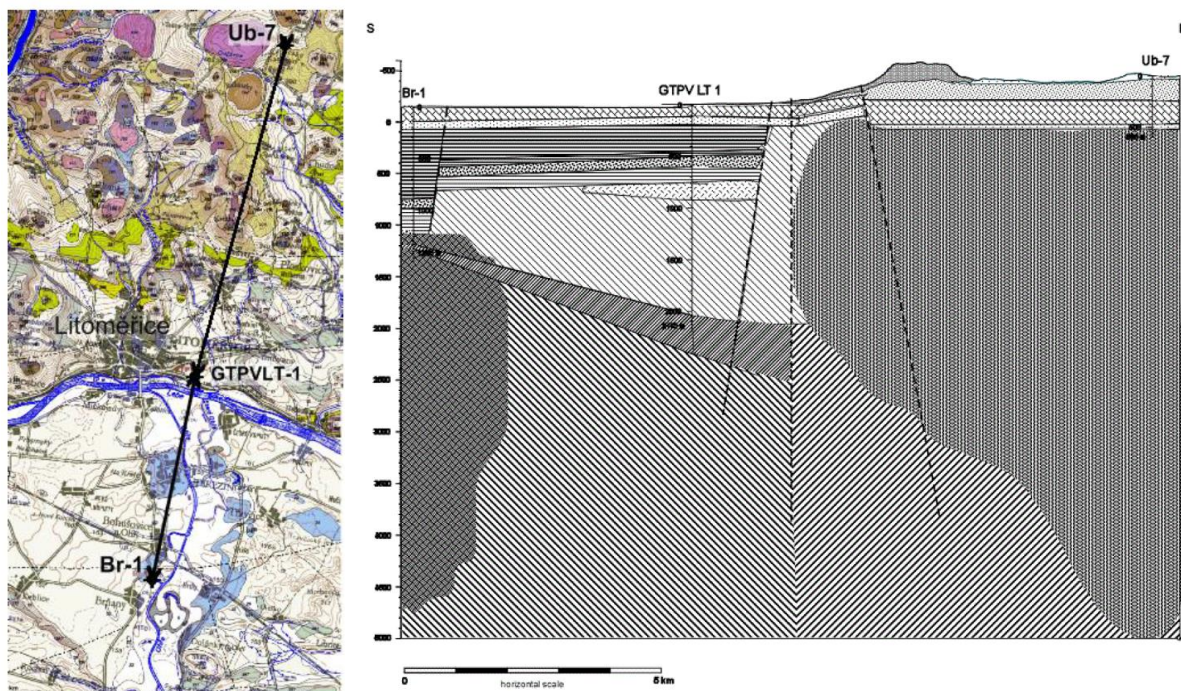

Figure 1 : Left: Borehole GTPV LT-1 in Litomerice and the position of the geological section running through them in the section of a geological map 1:50 000 published by the Czech Geological Survey. Right: Geological section from Br1 to Ub7.

2 MT Survey

2.1 Magnetoteotellurics in a periurban environment

2.1.1 Data processing techniques for noise removal

Magnetotellurics is a passive electromagnetic method based on synchronous measurements of both horizontal electric and magnetic fields time series, respectively E(t) and H(t) at ground surface. In frequency domain, the relationship between the electric and magnetic field components, respectively written E and H is defined by the equation

$$E = ZH \quad (1)$$

Where Z is a 2x2 frequency dependent tensor called the magnetotelluric impedance, from which apparent resistivity ρ_a (in Ωm) and phase tensor φ_a (in degrees) can be derived using the two following formulas:

$$\rho_a(f) = \frac{|Z(f)|^2}{\omega\mu_0} \quad (2)$$

$$\rho_a(f) = \arctan\left(\frac{imag(Z(f))}{real(Z(f))}\right) \quad (3)$$

where ω is the pulsation of the electromagnetic waves in rad.s^{-1} and μ_0 is the magnetic permeability of the void (SI).

The MT impedance tensor and associated apparent resistivity and phase tensors allows the MT user to investigate the geoelectrical properties of the subsurface in frequency domain. In electromagnetic methods, the depth of investigation of the electromagnetic waves is a function of the resistivity of the medium ρ and the frequency of observation f. In a homogeneous half space medium case of resistivity ρ, the depth of investigation δ (in m) is given by the so-called skin depth formula:

$$\delta = 503\sqrt{\frac{\rho}{f}} \quad (4)$$

Consequently, the depth of investigation increases when the frequency decreases.

MT natural sources covers the 1 mHz-10 kHz frequency band and are associated with external geomagnetic sources for frequencies under 1 Hz and atmospheric lightning (known as sferics) for frequencies above 1 Hz. Sources are assumed to be horizontal plane waves. The low frequency part of the MT sources allows to scan the subsurface up to tens of kilometers of depth, which is impossible with DC resistivity methods due to profile length limitations or controlled source electromagnetism (CSEM) methods because of transmitter limitations (by example, the maximum period of injected squared wave currents reachable with our Metronix transmitter TXM22 is 64 seconds).

Practically, a MT sounding consists in estimating frequency domain apparent phase and resistivity from recorded (E(t),H(t)). If the data were free of any noise, a simple least-square regression should be sufficient to solve equation (1) (Vozoff, 1972).

Unfortunately, MT sources are often polluted by anthropic electromagnetic sources especially in urban/peri-urban environments. The more sources, the less the signal to noise ratio. The closer the sources are from the MT stations, the less the plane wave assumption of MT is fulfilled. Noise sources can be permanent or transient at the scale of the measurements. When noise is transient and with duration less than half of the recorded time series, classical robust methods such as m-estimator and bounded influence estimator (Chave and Jones, 2012) can down weight anomalous data and a reliable Z estimate can be obtained.

Moreover, the noise sources can be local or global at the scale of the prospected area. Gamble et al. (1979) proposed the use of a distant (i.e. far from the prospect) remote reference station, recording magnetic field only, to filter the noise in the dataset during the estimation of Z. The justification of using magnetic signals instead of electric signals is that the amplitude of the telluric signals are strongly dependent on local geology, while the magnetic fields are coherent over many

kilometers as shown by Zelwer and Morrison (1972). The limit of this so-called Remote Reference Method is that if correlated noise is present on both local and remote magnetic data, it won't be filtered by the method and a biased Z estimate will be obtained. In addition, if the local electric field is entirely saturated by local noise, the remote reference processing should fail.

2.1.2 Geomedia's 2006 NS MT profile

In 2006, a MT survey was performed in the context of geothermal exploration in the Litomerice area by Geomedia. A 3.5 km long NS profile of 11 MT station was performed across the Elbe river (*Figure 2*). Despite the use of a local (15 km away) and a distant (geomagnetic observatory data in Budkov u Prachatic, 200 km away) Remote Reference station and robust processing, MT soundings were strongly biased at low frequencies.
Bias on apparent resistivity and phase profiles is illustrated by an asymptotic behavior of the curves at low frequency:
- the resistivity increase linearly with decreasing frequency, the increasing rate is approximately one decade of resistivity increase by one decade of frequency decrease
- Apparent phase tends to 0 degrees when frequency decreases.

Geomedia (2006) concluded that such phenomenon was linked to a grounded horizontal dipole in the vicinity of the profile. This dipole could be connected to the EW railroad, crossing the profile on the North side of the Elbe River.
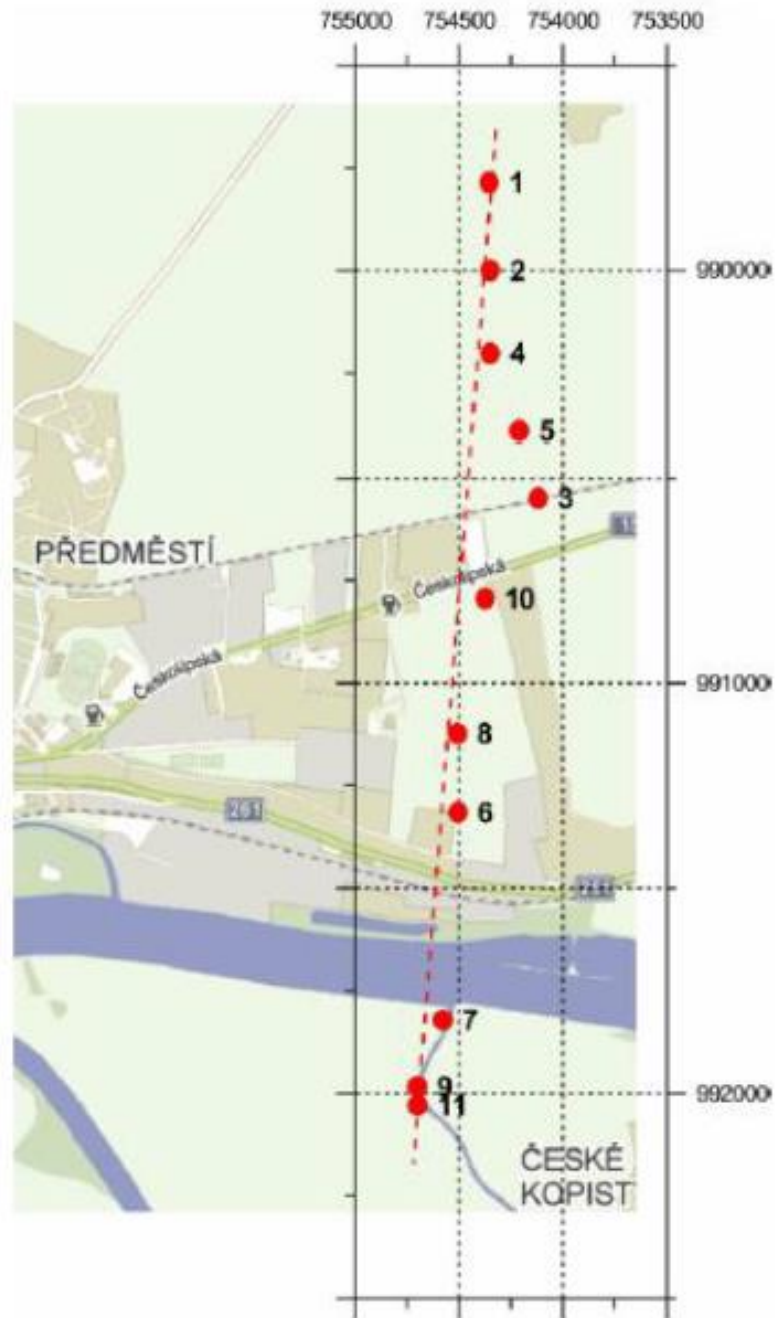
Figure 2 : MT station locations from Geomedia NS MT profile (extracted from Geomdia report, 2006)
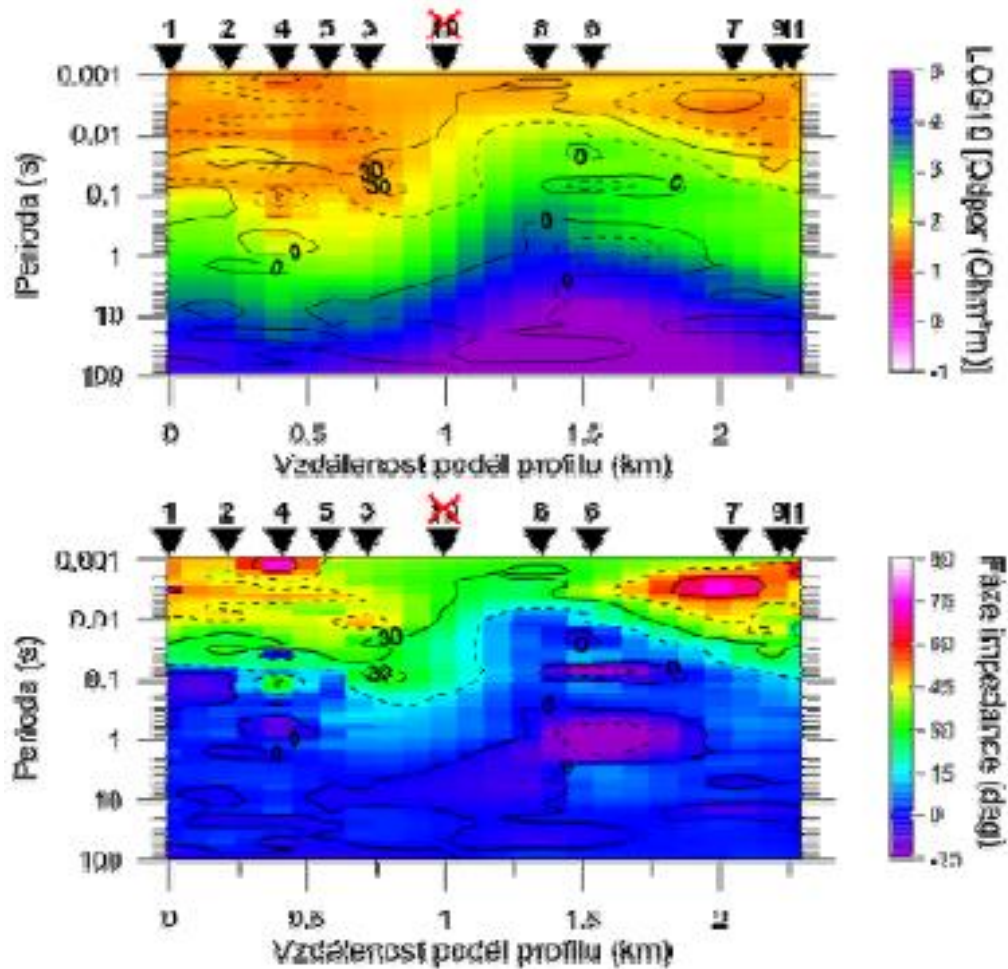
Figure 3: Geomedia's MT pseudo-sections along the profile (North to South), xy component of the impedance tensor: i) upper pannel: apparent resistivity in log10 scale (in Ω.m), i) lower pannel: apparent phase

2.1.3   The BRGM MT campaign in September 2014

In the framework of the Image project and on the sidelines of the CSEM survey, the BRGM conducted a MT campaign along the Northern part of the Elbe River, repeating the NS profile acquired by Geomedia. As shown in Figure 4, the BRGM profile was constituted of 7 MT sites, named MT06 to MT12, which were also investigated in CSEM configuration (see the next section for more details). The scientific purpose was to use i) new acquisition setups (MT stations ADU07, designed by Metronix) ii) 2 Remote Reference stations located at approximately 25 km on the east and on the western side of the profile (respectively named REF1E et REF2W) and iii) new robust processing techniques to reduce the bias on the low frequency part of the MT soundings.
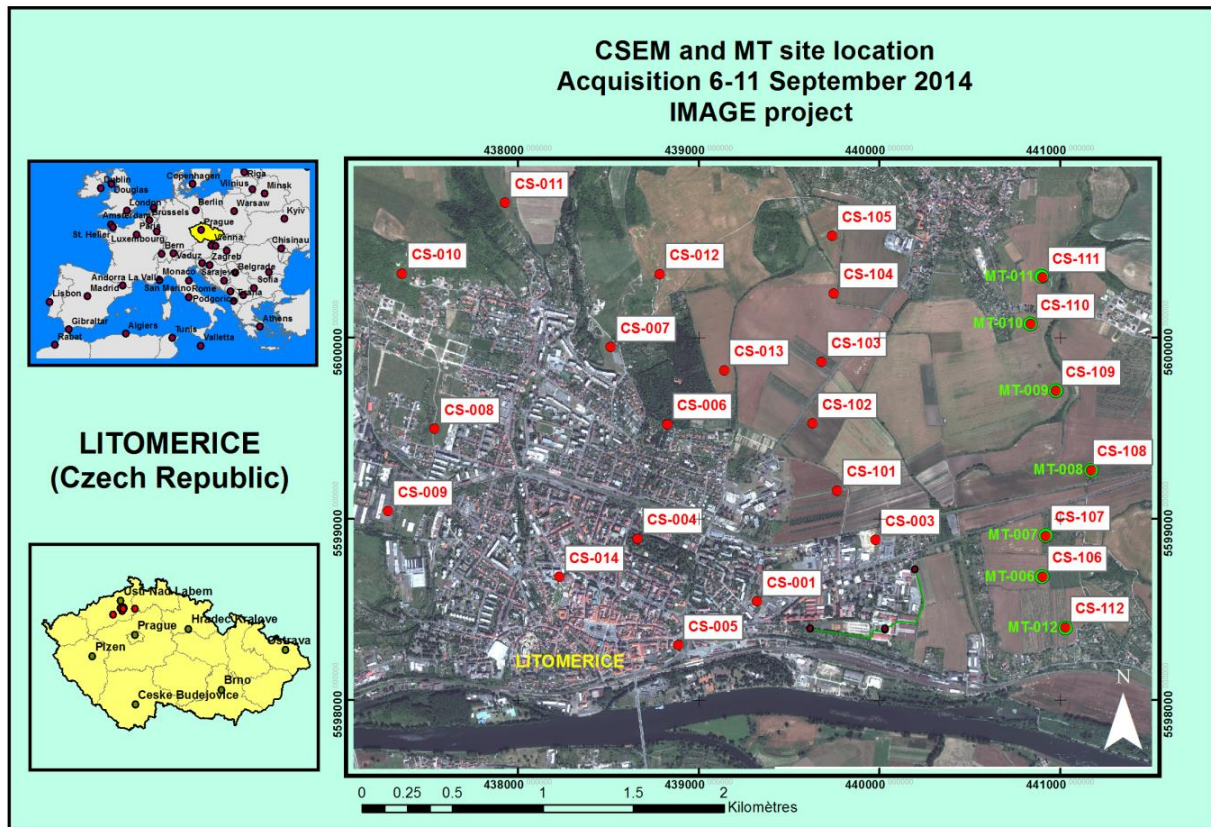
Figure 4: BRGM survey in 2014. CSEM and MT station locations in the Litomerice area. MT sites are indicated in green on th eastern site of the prospect. Eastern and Western Remote Reference stations are located 25km away form the profile and shown in red dots on the down left pannel.

The time schedule of the survey is summarized in Figure 5. Each site was investigated using two sampling frequencies: 128 Hz (MT data of at least 10 hours duration) and 4096Hz (MT data of 1h). Processing of both time series allows the estimation of Z, apparent resistivity and phase from 10 mHz to 1 kHz.

The western remote reference was that used only for the first day of the MT survey, consequently, only site 10 was synchronous with both REF1E and REF2W. All other stations were synchronous with REF1E only.
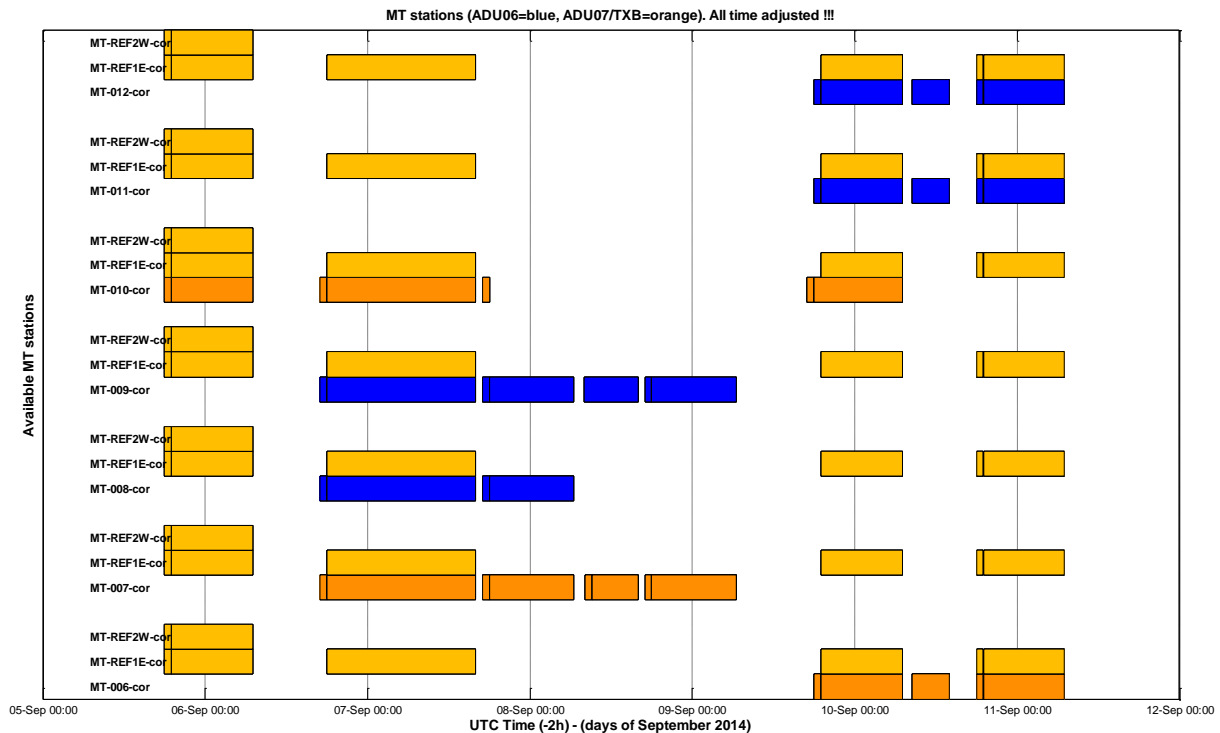
Figure 5: Time schedule of MT acquisition along the BRGM profile: each block represents represents a period of measurements, long blocks corresponds to 128 Hz sampling MT data (at least 10 hours) while small blocks corresponds to 1h hour long MT data at 4096Hz.

2.1.4 Robust Processing techniques and time lapse approach

Let us consider E, H and H^R as the electric field, the magnetic field and the reference magnetic fields.

All site data were processed using different robust techniques:

- Classical Robust single site processing, without use of any remote reference magnetic signals: this relies on the M-estimator (Chave and Jones, 2012, Chapter 5.5), which is a weighted least-square approach to solve Z in equation 1. The M estimator minimizes the influence of data associated with large residuals on Z estimates.
- Bounded Influence (BI) Estimator processing (Chave and Jones, 2012, Chapter 5.6), includes the M-estimator but also minimize the influence of extreme values in the magnetic fields, also called *leverage points*.
- Classical Robust Remote Reference processing, using the M-estimator again.
- Two-stage Bounded Influence estimator. First, the following equation is solved for Q using Bounded Influence estimator:

$$H = QH^R \ (5)$$

Then, a predicted magnetic field is constructed with H^R and Q, such as $H^P = QH^R$ and equation (1) is solved for Z by substitution of H by H^P using the BI estimator.

All of these techniques were applied providingan impedance estimate $Z^{est}(f)$ and its associated error $\Delta Z^{est}(f)$ for frequencies ranging between 10^{-2} Hz to 10^3 Hz.

In order to deal with long duration transient noise events that could affect frequency bands, we assumed a time-lapse approach for our MT processing. Each time series (E(t),H(t)) were divided in successive windows of 2^{19} samples, and processed for 48 frequencies starting from half the Nyquist frequency (named f_N) to f_N/64 leading for each frequency to a number N_{est} of consecutive estimates of $Z(f_{est})$ and its associated errors $\Delta Z(f_{est})$. Each

consecutive processing results is associated with the middle time of its time window, named thereby t_{est}.

The observation in the time-frequency plane of $Z(f_{est}, t_{est})$, $\Delta Z(f_{est}, t_{est})$ and associated apparent resistivity and phase $\rho(f_{est}, t_{est})$, $\varphi(f_{est}, t_{est})$ is a useful way to assess the stability of the impedance estimates and to characterize transient or long duration noise sources. Let us consider the case of a 12 hours long dataset at 128Hz sampling data measured on site 9.
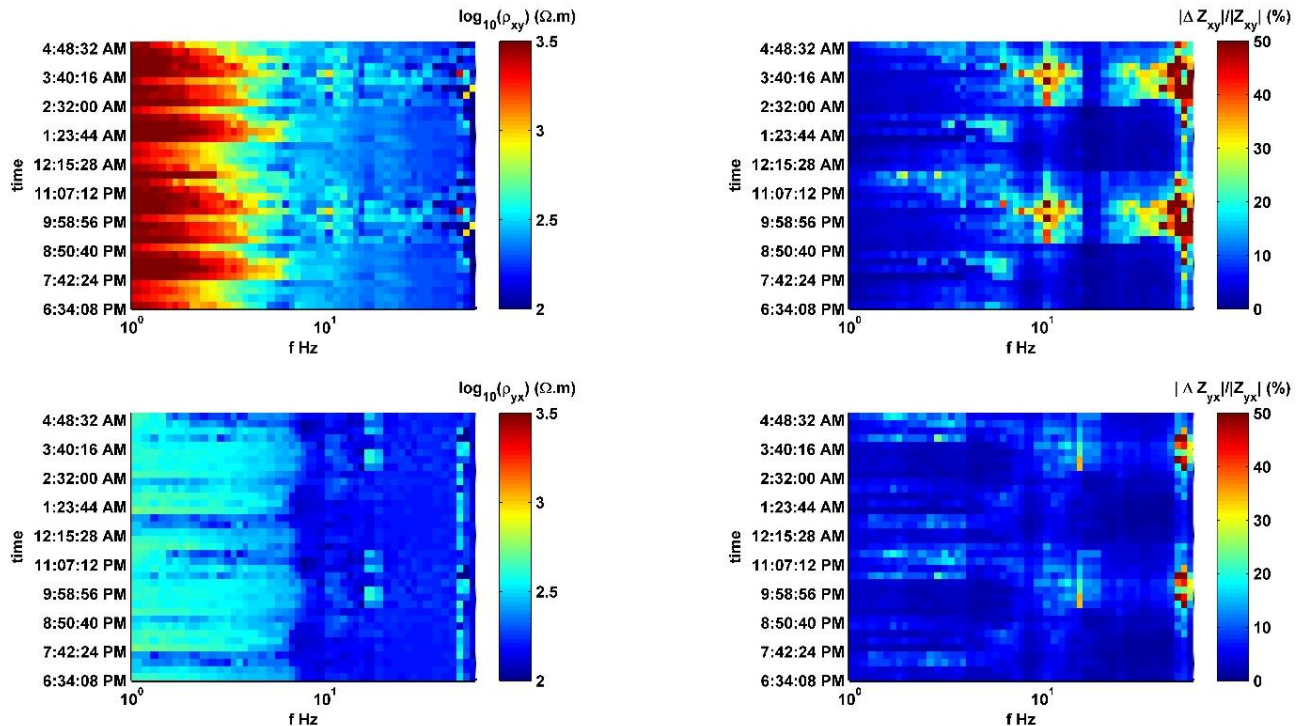
Figure 6: Site 9, 128hz sampling time series from 06/09/2014, processed with remote reference REF1E. Time-Lapse observation of apparent resistivity $\rho_{XY}(f_{est}, t_{est})$ and $\rho_{YX}(f_{est}, t_{est})$ in log10 scale (respectively left pannel up and down) compared to relative error $\Delta Z_{XY}(f_{est}, t_{est})$ and $\Delta Z_{YX}(f_{est}, t_{est})$ (respectively right pannel up and down).

Figure 6shows in the time-frequency plane the variation of apparent resistivity estimates $\rho_{XY}(f_{est}, t_{est})$ and $\rho_{YX}(f_{est}, t_{est})$ for a 128Hz 10 hours long time series (from 06-7/09/2014) and compares it with associated relative error estimates on the impedance $\Delta Z_{XY}(f_{est}, t_{est})$ and $\Delta Z_{YX}(f_{est}, t_{est})$. Significant time variations of apparent resistivity are observed on XY in time for a a large number of frequency. Focusing on frequencies above 10 Hz, time scatter appears between 8:50pm and 0:0 AM, and later between 2:30 and 4:00 AM. This time scatter is correlated in time and frequency with large error values on $\Delta Z_{XY}(f_{est}, t_{est})$.

On the YX component, similar behavior is observed but with lower amplitude. At 15Hz, resistivity estimates becomes larger between 8:50pm and 0:0 AM, and later between 2:30 and 4:00 AM. Again, this behavior is correlated with larger error estimates on $\Delta Z_{YX}(f_{est}, t_{est})$. On the lower frequencies (f<5 Hz), negative variations of resistivity are correlated with higher values of errors while on the XY component, positive variations of resistivity are correlated with large errors.

Let us now test the hypothesis that portions of the time-frequency domain associated with large relative errors are associated with transient and/or pseudo-periodic noise sources. We selected the 50% "best" (hereafter **min ΔZ**) estimates associated with the lower relative error values and the 50% "worst" (hereafter **max ΔZ**) estimates (associated with time periods between 8:50 pm and 0:0 AM, and later between 2:30 and 4:00 AM). Then, a simple median is conducted on the populations of best and worst $Z(f_{est}, t_{est})$ estimates leading to an apparent resistivity and phase sounding shown on Figure 7.

It is obvious that the **max ΔZ** sounding shows unstable and noisy apparent phases on both components xy and yx. The **min ΔZ** sounding shows less scatter on the apparent resistivity but for

frequencies under 10Hz, xy phases tends to 0° and both xy and yx resistivity enters in higher resistivity regime (a minimum jump of factor 2 is observed at low frequencies). This behavior is non-physical in the scope of MT laws, and can only be explained by the presence of a stationary electromagnetic source in the vicinity of the MT station.

Our conclusion is that filtering the time lapse estimates of MT impedance $Z(f_{est}, t_{est})$ using relative errors $\Delta Z (f_{est}, t_{est})$ amplitude as quality criterion allows to obtain smoother MT soundings by filtering estimates corrupted by transient noise sources but fails in filtering biased estimates, linked with the presence of a permanent/pseudo-permanent noise source present on both remote reference magnetic data and MT site electric and magnetic data.

The low frequency bias shown on site 09, located in the middle of the MT profile can be observed on all MT soundings of the profile, whatever the processing type such as observed by Geomedia in 2006. The direct consequence of this low frequency noise is that MT soundings cannot be exploited below 5Hz.

Figure 7: Site 9, 128 Hz sampling time series from 06/09/2014, processed with remote reference REF1E. Compared apparent resistivity and phase component estimates XY and YX.

2.1.5 N-S MT profile

In this section, we compare MT soundings obtained from Bounded influence robust processing (Chave and Jones, 2012) for both Single Site processing and Remote Reference processing using the 25 km away REF1E station.

At first, a sounding by sounding analysis is performed by comparing SS an RR apparent resistivity and phases. In a general way SS processing soundings are strongly different from RR soundings at frequencies above 1Hz on both apparent resistivity and phase. As shown on sounding MT10 inFigure 8, apparent resistivity issued from RR are smoother and more coherent above 1 Hz than SS ones, despite a biased frequency band around 50 Hz. Above 1 Hz again, RR phases differs strongly from SS ones but are very noisy on the yx component. Below 1 Hz, xy phases tends to 0° at low frequency and xy resistivity tends to an asymptotic behavior, which reveals the pollution of MT data by close noise source, as suggested by Geomedia in 2006.

In order to estimate the degree of reliability of the MT dataset above 1 Hz, we compared for site 10 and for each frequency band our apparent resistivity tensor $\rho_a^{MT}(f)$ to the equivalent half-space resistivity derived from the CSEM data: $\rho_a^{CSEM}(f)$ (shown in green on Figure 8, explanations on how to derive this quantity is given in the CSEM section). A good match is obtained between $\rho_a^{CSEM}(f)$ and the xy component of $\rho_a^{MT}(f)$ above 5 Hz and with both xy and yx above 30 Hz. This site is located 2km away from the CSEM source i.e. roughly three skin-depth at 10Hz. We can therefore assume that at this site and above 10Hz, CSEM data are Controlled Source Audio MT data (CSAMT) and resistivities obtained CSEM and MT should be similar. This demonstrates that MT data above 5Hz are trustworthy.

In addition, a synthetic MT 1D sounding (ρ_a^{1D},φ_a^{1D}) was created from the resistivity logs from the nearest borehole (shown in the next CSEM section again, shown in black on Figure 8). At frequencies above 5 Hz, the fit is good to very good between xy and yx components of $\rho_a^{MT}(f)$ and ρ_a^{1D} (f). The fit is good on the apparent phases above 30 Hz.

From the comparison with CSEM and borehole data, we conclude that the quality of our RR MT estimates is good above 10 Hz, despite significant noise on the yx phases. Unfortunately, below 5 Hz, MT soundings are corrupted by an anthropic noise source that cannot be eliminated with RR processing. Site MT10 (Figure 8) is representative of the overall behavior and quality of MT soundings of the profile while data quality decreases southwards, towards railways.
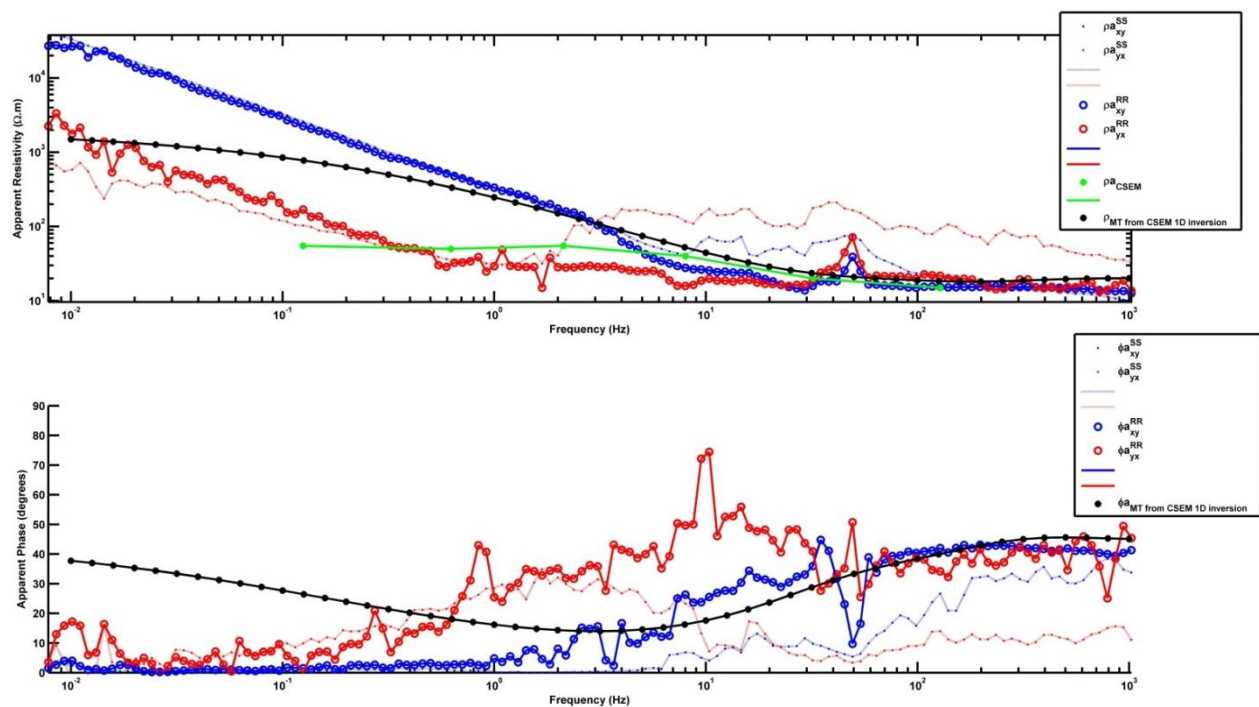
Figure 8: Site MT10 apparent resistivity (upper pannel) and phases (lower pannel) for components xy (blue) and yx (red) as a function of frequency for Single Site processing (dashed lines and points) and Remote Reference Processing (full lines and circles). Comparison is made with CSEM apparent resistivty sounding (green line) for the same site and with a synthetic MT sounding (black lines and dots constructed from a 1D resistivity model issued from CSEM 1D inversion (see next section).

RR and SS MT data are summarized on apparent resistivity pseudo sections (apparent resistivity as a function of frequency and offset along the MT profile) on Figure 9 for both anti-diagonal components ρ_{xy}^{MT} and ρ_{yx}^{MT}, and also from the 1D equivalent apparent resistivity associated with the determinant of the impedance tensor Z, and hereafter written ρ_{1D}^{MT}. Despite the corrupted site MT06 and the lack of remote reference data on frequencies above 64 Hz for sites MT07 to MT09,

comparison between SS and RR pseudo-section shows that RR results are smoother than SS ones or frequencies above 1Hz especially on the yx component. These pseudo-sections also show the global presence of the low frequency asymptote on both xy and yx.
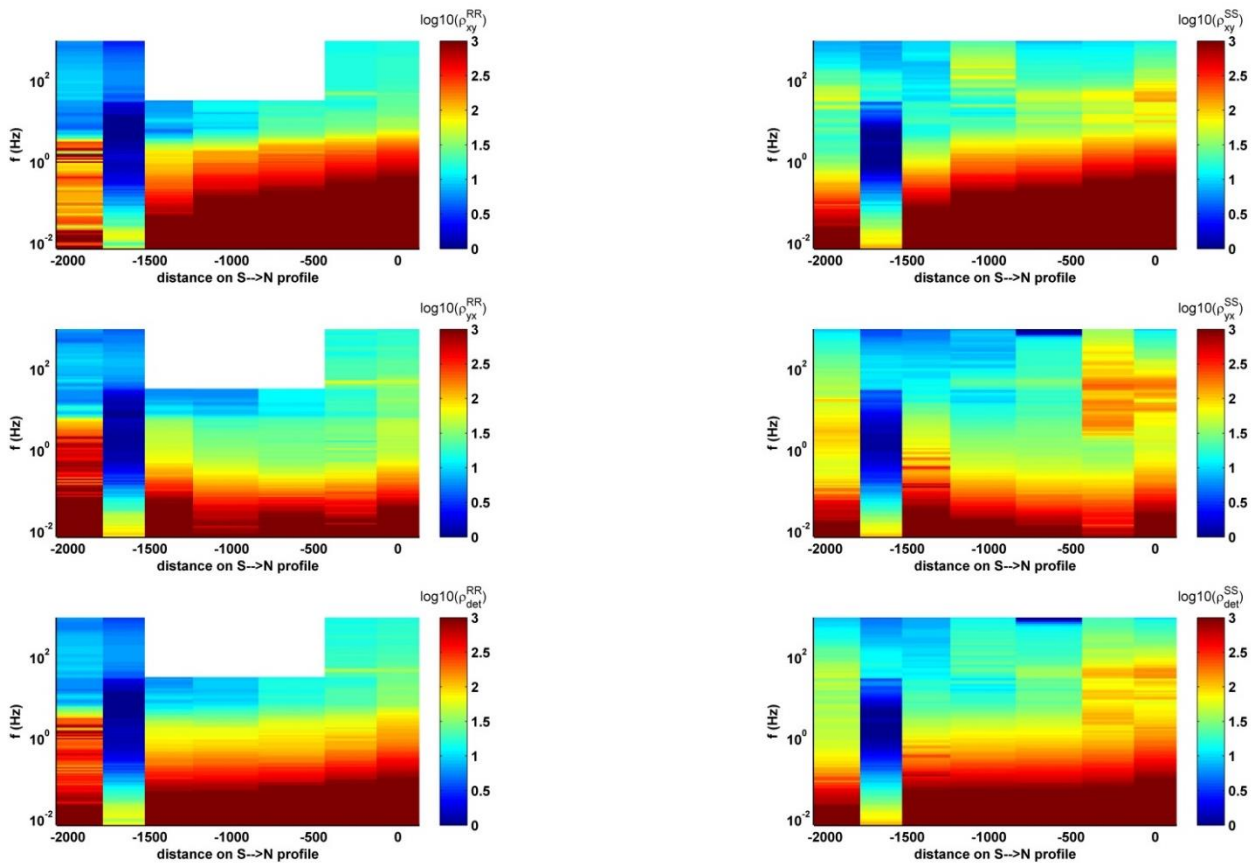
Figure 9: South to North profile of apparent resistivity pseudo profile in log$_{10}$ scale and in Ω.m for RR processing results (left pannel) and SS processing results (right pannel), for xy component (upper pannel), yx component (middle pannel) and 1D equivalent/determinant (lower pannel). The northern site is at abscissa 0, southern sites have negative abscissa. Blanked areas on RR pseudo-profiles are shown when no synchronous remote data was available to process frequencies above 64Hz.

Apparent phase pseudo profiles were also constructed for xy and yx on Figure 10. They show that RR phases are significantly higher than SS ones at frequencies above 5Hz but tends to 0° below 5Hz. Moreover, the two southern sites (respectively 12 and 6) display noisy phases on RR processing results.
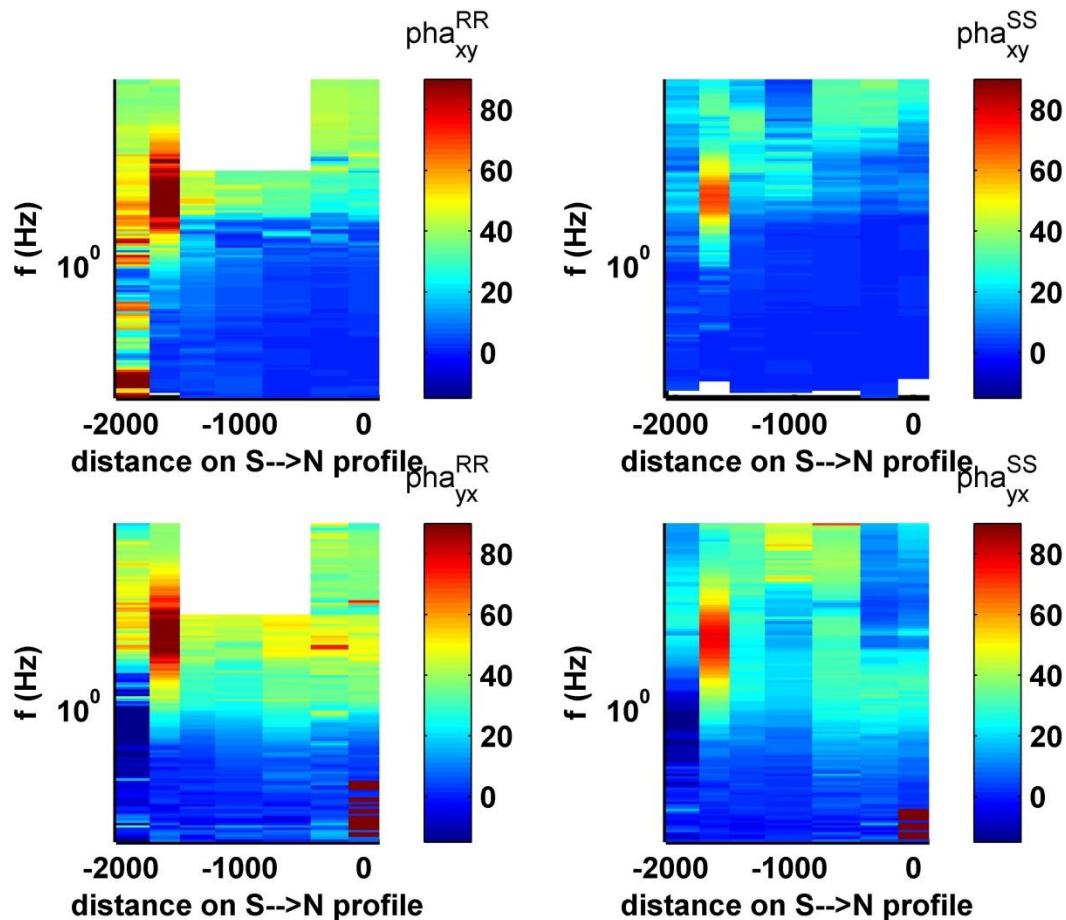
Figure 10: South to North profile of apparent phase pseudo profile degrees for RR processing results (left panel) and SS processing results (right panel), for xy component (upper panel), yx component (lower panel). The northern site is at abscissa 0, southern sites have negative abscissa. Blanked areas on RR pseudo-profiles are shown when no synchronous remote data was available to process frequencies above 64Hz.

2.1.6 Conclusions on the MT survey

Despite the use of a remote reference, MT data are corrupted at low frequency by a permanent anthropic noise source. Transient anthropic noise sources bias are partially filtered/eliminated using a time lapse approach based on error thresholding. Then, RR processing smooth the MT soundings but their low frequency part still behave in an asymptotic way, traducing the presence a near field source that forbids MT source properties to be fulfilled. A comparison with CSEM data has been performed and shows that MT data are trustworthy at high frequencies (above 10 Hz). A second comparison has been performed between MT soundings and a synthetic 1D sounding based on borehole resistivity logs. The fit is very tight on the northern part of the profile for frequencies above 5 Hz, while further South, noise sources forbids the use of MT quantities. Both comparisons assess the quality of our "denoising" techniques for MT soundings at frequencies above 5-10 Hz on the northern part of the profile. Meanwhile, CSEM should be more appropriated for peri-urban areas, especially in MT frequency bands corrupted by anthropic sources.

3 CSEM Survey

3.1 Crew, Equipment and Survey Plan
The CSEM survey took place from the 6th until the 11th of September over the Litomerice geothermal area.

3.1.1 Crew
The CSEM survey required to following BRGM staff:
- 3 geophysicists and :
    - Nicolas Coppo
    - Jean-François Girard
    - François Benjamin
    - Robin Barbier
- as well as the Geomedia staff:
    - Hana Jirakova
    - Vaclav Frydrych

3.1.2 Equipment
The equipment used during the survey was:
Transmitter (TX) :
- 1 50 kVA power generator
- 1 TXM 22 et 1 TXB07 (Metronix, Germany)
- 1 isolation transformer
- 50 metallic sticks (electrodes)
- 600 m of cable
- Cables and material
- 1 vehicule

Receivers (RX) and remote references:
- 3 MT stations Metronix (Germany) including
    - 1 ADU07 (Metronix, Germany)
    - 2 magnetic sensors (MFS07 or MFS07e)
    - 5 non polarisables electrodes
    - 1 battery
    - GPS, compas, level, shovel, pickaxe
    - Water tank
    - Material
- 1 differential GPS
- 3 vehicles
- Battery chargers

3.1.3 Survey log

04/09/2014
Arrival at Litomerice of BRGM staff (JF & NC)

Field excursion with Hana Jirakova (Geomedia), Vaclav Frydrych (Geomedia) and Antonin Tym (Litomerice City) to check expected acquisition sites.

05/09/2014

Delivery of the power generator at the injection borehole.
Field tour to find location for 2 MT remote references.
Arrival at Litomerice of BRGM staff (BF & RB) with geophysical equipment.
Set up of the two references, together with MT10 (cimetary), with the following recording sequence

- 1x 4096 Hz pendant 59 min
- 1x 128 Hz from 9 PM until 9 AM

06/09/2014

Set up of the cables and electrodes for the current injection (TXM22) along two dipoles.
Set up of 3 new MT stations (MT07- MT08- MT09 in addition to MT10)
Acquisition of CSEM data: CS110 and CS107 at 4 PM. Injection problem.
CSEM recordings interrupted on stations MT07 to MT09 during the first run at 0.125Hz, and recovered on transmitting dipole 2 at 0.5 Hz.

07/09/2014 - OFF

Quality check.

08/09/2014

CSEM data acquisition (CS001, CS003, CS004, CS005, CS006, CS007, CS014).

09/09/2014

CSEM data acquisition (CS008, CS009, CS010, CS011, CS012, CS013, MT110).
Set up of 3 new MT stations (MT11, MT12 and MT06) on the eastern profile.

10/09/2014

CSEM data acquisition on 3 MT stations installed Tuesday evening 09/09/2014 (MT profile)
-    CS111, CS106, CS112

CSEM data acquisition (CS101, CS103, CS102, CS104, CS105).

11/09/2014

Demobilization.

3.2 Field Setup and Transmitter Sequences

3.2.1 Transmitter location (TX)

The transmitter was installed in the South-East corner of the Litomerice city (Figure 11) next to the 2006 geothermal exploration well (Figure 12).
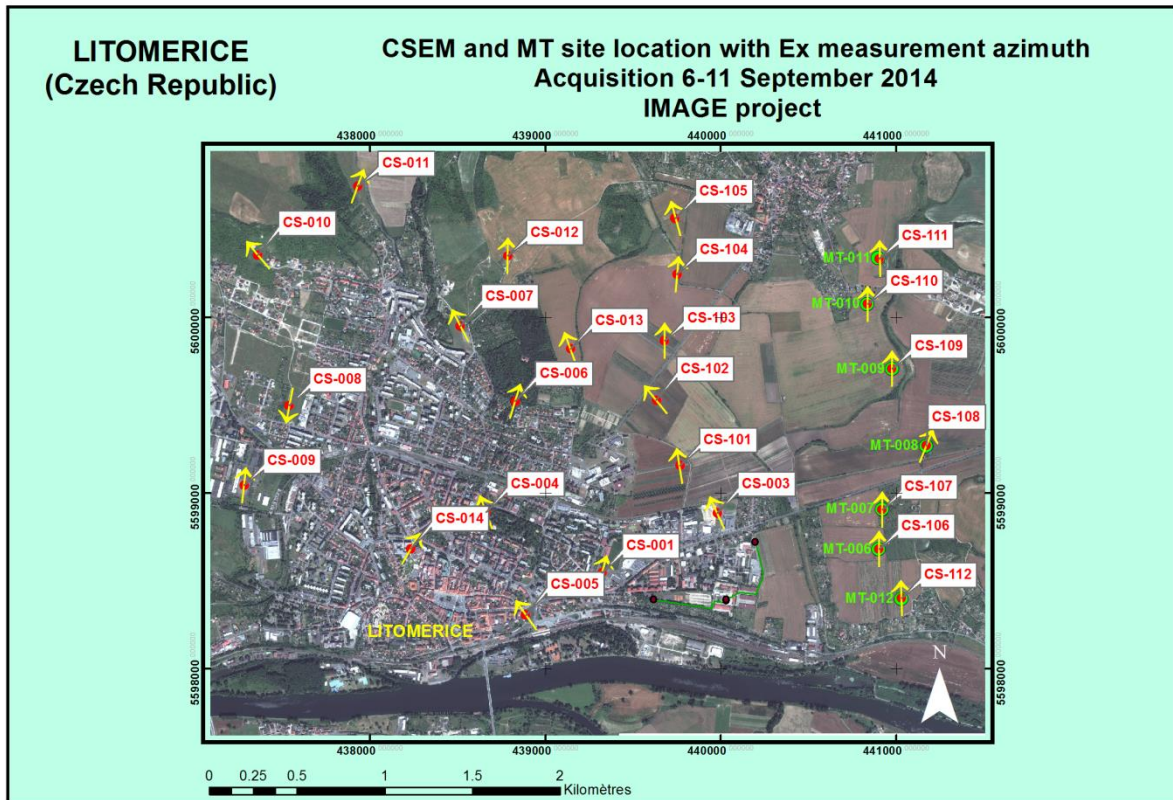
Figure 11 – Location of the transmitter (green lines) and receivers (red dots). On the eastern part is shown the MT profil (stations MT06-MT12, in green).

Figure 12 - Location of current injection poles. U and V are surface injection points and W is a 1.8 km long metallic casing borehole (Google Earth image).

The transmitter consists in two electrodes (E1 and E2) and one 1.8km long metallic casing (E3) with E2 roughly at 90 degrees from E1. Coordinates of the injection points are given on Table 1. This allows injecting current in three different dipoles (E1-E2, E1-E3 and E2-E3). Because the transmitter is able to use there electrodes at the same time to define any current vector, we had to

choose two distinct polarizations in order to reduce current close to 0A alternatively on E1 and E2. The two polarizations used were:

Polarization	Azimuth (approx.)	Polarization angle	
POL-1W	~270°N → West	30°	
POL-2N	~15°N → North	90°	
POL-3NE	~55°N → North-East	150°	Not used

Every surface injection point is made of roughly 12 electrodes (Figure 13). For the borehole injection point, a cable is screwed on the wellhead (Figure 14) then connected to a Metronix transmitter TXM22 with TXB07 controller powered by a 50 kVA power generator (Figure 16). This equipment allows injecting any type of current between 0.03125 Hz and 16384 Hz. As this transmitter provides a constant output voltage (~540 V) and maximum power of 22 kW, only the lowering the ground resistance allows to maximize the injected current (as U=RI). If the shallow layers are very conductive (~15 Ωm) or using boreholes, injected current can reach 40 A in the best configurations.

	UTM 33N coordinates (WGS84)		
Electrode	Easting (m)	Northing (m)	Elevation (m)
E1 (U) W	439616	5598393	169
E2 (V) N	440191	5598721	174
E3 (W) Borehole	440023	5598389	172

	Distance (straight line, in m)
E3-E1	407
E3-E2	371
E1-E2	662

Table 1 : Coordinates of the injection points

Figure 13 : Surface electrode (E1).

Figure 14 : Borehole head with electrical connection.

Figure 15 : Transmitter TXM22 with TXB07 controller.

Figure 16 : 50 kVA power generator.

3.2.2   Receiver layout (Rx)

25 CSEM stations recording both electric and magnetic fields have been deployed to cover the Litomerice area (Figure 17). The stations have been synchronized by GPS to the transmitter. Electric and magnetic fields have been measured using two 100m long perpendicular electric dipoles (Ex and Ey) and two horizontal magnetics coils (Hx and Hy), respectively (Figure 18 et Figure 19).
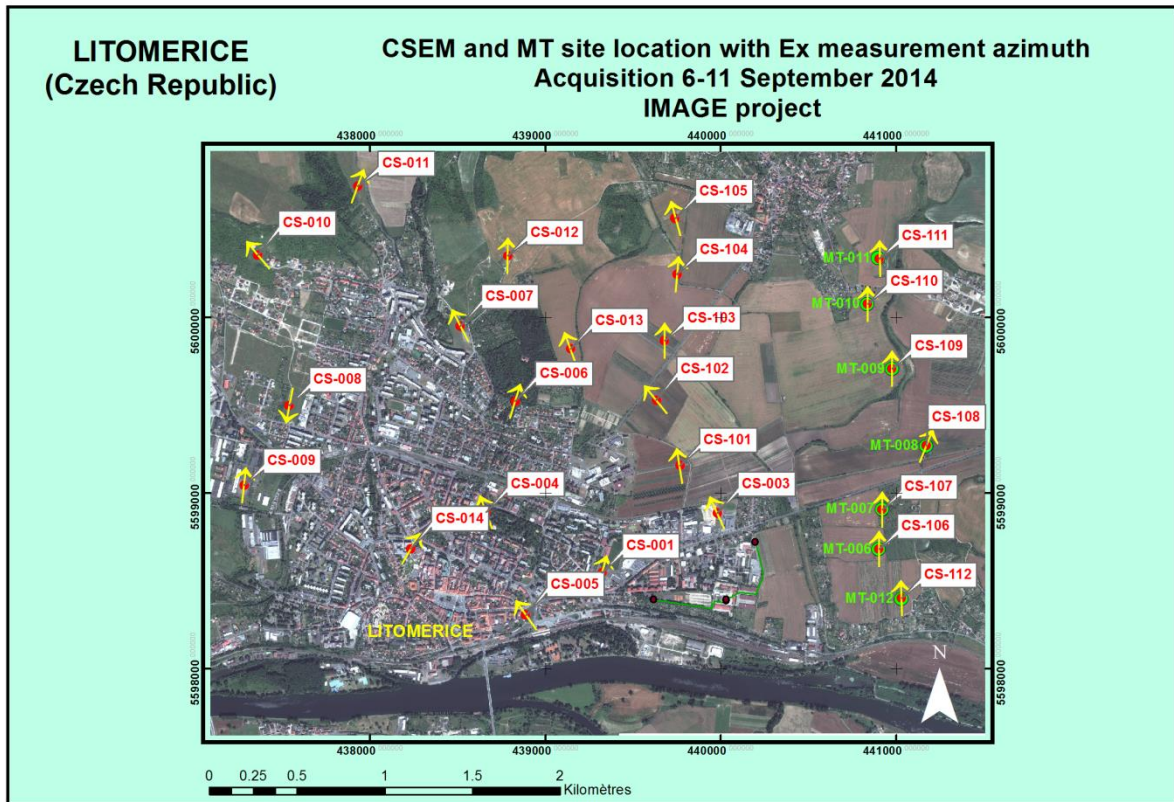
Figure 17 : CSEM stations as well as MT stations.
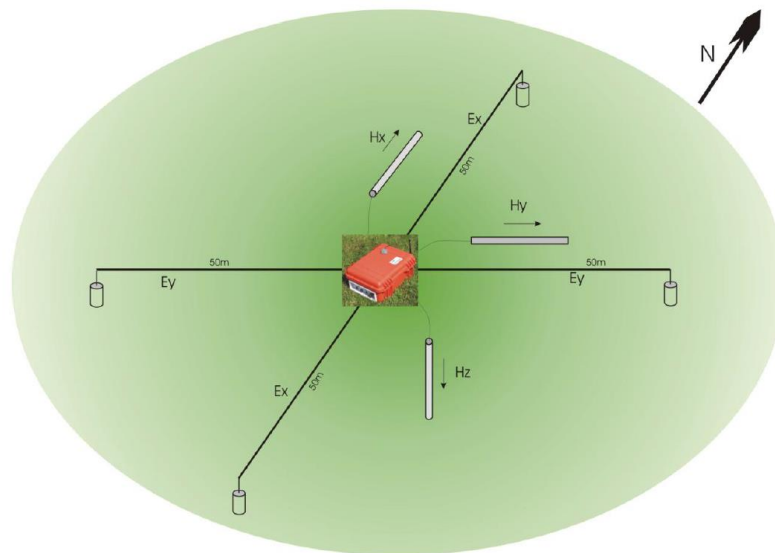
Figure 18 : Receiver setup.

Figure 19 : Recording device (ADU07 in orange)

3.2.3 Transmission frequencies

Current injections have been performed alternatively on both electric source dipoles (POL 1 and POL 2) with varying fundamental frequencies (0.125 – 0.5 – 2 – 8 – 32 -128 Hz, see Table 2). The waveform was as a square wave to maximize signal/ratio at the fundamental frequency and odd harmonics (Figure 20 :).

Frequencies (Hz)	Duration (mn)
0.125	15
0.5	5
2	4
8	3
32	2
128	1

Table 2 : Transmission frequencies and duration for each dipole orientation

Figure 20 : Monitored current (128 Hz) on the 3 electrodes when using POL-1W, with 1Hz rectangular signal waveform. Current goes mainly between E1 and E3 (borehole).

SiteName	Fundamental	POL	Time
site001	0.125Hz	1W	2014-09-08_14-00-00
site001	0.5Hz	1W	2014-09-08_14-16-00
site001	2Hz	1W	2014-09-08_14-21-00
site001	8Hz	1W	2014-09-08_14-24-00
site001	32Hz	1W	2014-09-08_14-26-00
site001	128Hz	1W	2014-09-08_14-28-00
site001	0.125Hz	2N	2014-09-08_13-00-00
site001	0.5Hz	2N	2014-09-08_13-16-00
site001	2Hz	2N	2014-09-08_13-21-00
site001	8Hz	2N	2014-09-08_13-24-00
site001	128Hz	2N	2014-09-08_13-28-00
site003	0.125Hz	1W	2014-09-08_14-00-00
site003	0.5Hz	1W	2014-09-08_14-16-00
site003	2Hz	1W	2014-09-08_14-21-00
site003	8Hz	1W	2014-09-08_14-24-00
site003	32Hz	1W	2014-09-08_14-26-00
site003	128Hz	1W	2014-09-08_14-28-00
site003	0.125Hz	2N	2014-09-08_13-00-00
site003	0.5Hz	2N	2014-09-08_13-16-00
site003	2Hz	2N	2014-09-08_13-21-00
site003	8Hz	2N	2014-09-08_13-24-00
site003	128Hz	2N	2014-09-08_13-28-00
site004	0.125Hz	1W	2014-09-08_11-00-00
site004	0.5Hz	1W	2014-09-08_11-16-00
site004	2Hz	1W	2014-09-08_11-21-00
site004	8Hz	1W	2014-09-08_11-24-00
site004	32Hz	1W	2014-09-08_11-26-00
site004	128Hz	1W	2014-09-08_11-28-00
site004	0.125Hz	2N	2014-09-08_13-00-00
site004	0.5Hz	2N	2014-09-08_13-16-00
site004	2Hz	2N	2014-09-08_13-21-00
site004	8Hz	2N	2014-09-08_13-24-00
site004	128Hz	2N	2014-09-08_13-28-00
site005	0.125Hz	1W	2014-09-08_15-00-00
site005	0.5Hz	1W	2014-09-08_15-16-00
site005	2Hz	1W	2014-09-08_15-21-00
site005	8Hz	1W	2014-09-08_15-24-00
site005	128Hz	1W	2014-09-08_15-28-00
site005	0.125Hz	2N	2014-09-08_15-50-00
site005	0.5Hz	2N	2014-09-08_16-06-00
site005	2Hz	2N	2014-09-08_16-11-00
site005	8Hz	2N	2014-09-08_16-14-00
site005	32Hz	2N	2014-09-08_16-16-00
site005	128Hz	2N	2014-09-08_16-18-00
site006	0.125Hz	1W	2014-09-08_16-20-00
site006	0.5Hz	1W	2014-09-08_16-36-00
site006	2Hz	1W	2014-09-08_16-41-00
site006	8Hz	1W	2014-09-08_16-44-00
site006	32Hz	1W	2014-09-08_16-46-00
site006	128Hz	1W	2014-09-08_16-48-00
site006	0.125Hz	2N	2014-09-08_15-50-00
site006	0.5Hz	2N	2014-09-08_16-06-00
site006	2Hz	2N	2014-09-08_16-11-00
site006	8Hz	2N	2014-09-08_16-14-00
site006	32Hz	2N	2014-09-08_16-16-00
site006	128Hz	2N	2014-09-08_16-18-00
site007	0.125Hz	1W	2014-09-08_16-20-00
site007	0.5Hz	1W	2014-09-08_16-36-00
site007	2Hz	1W	2014-09-08_16-41-00
site007	8Hz	1W	2014-09-08_16-44-00
site007	32Hz	1W	2014-09-08_16-46-00
site007	128Hz	1W	2014-09-08_16-48-00
site007	0.125Hz	2N	2014-09-08_15-50-00
site007	0.5Hz	2N	2014-09-08_16-06-00
site007	2Hz	2N	2014-09-08_16-11-00
site007	8Hz	2N	2014-09-08_16-14-00
site007	32Hz	2N	2014-09-08_16-16-00
site007	128Hz	2N	2014-09-08_16-18-00
site008	0.125Hz	1W	2014-09-09_11-30-00
site008	0.5Hz	1W	2014-09-09_11-46-00
site008	2Hz	1W	2014-09-09_11-51-00
site008	8Hz	1W	2014-09-09_11-54-00
site008	32Hz	1W	2014-09-09_11-56-00
site008	128Hz	1W	2014-09-09_11-58-00
site008	0.125Hz	2N	2014-09-09_11-00-00
site008	0.5Hz	2N	2014-09-09_11-16-00
site008	2Hz	2N	2014-09-09_11-21-00
site008	8Hz	2N	2014-09-09_11-24-00
site008	32Hz	2N	2014-09-09_11-26-00
site008	128Hz	2N	2014-09-09_11-28-00
site009	0.125Hz	1W	2014-09-09_14-00-00
site009	0.5Hz	1W	2014-09-09_14-16-00
site009	2Hz	1W	2014-09-09_14-21-00
site009	8Hz	1W	2014-09-09_14-24-00
site009	32Hz	1W	2014-09-09_14-26-00
site009	128Hz	1W	2014-09-09_14-28-00
site009	0.125Hz	2N	2014-09-09_13-30-00
site009	0.5Hz	2N	2014-09-09_13-46-00
site009	2Hz	2N	2014-09-09_13-51-00
site009	8Hz	2N	2014-09-09_13-54-00
site009	32Hz	2N	2014-09-09_13-56-00
site009	128Hz	2N	2014-09-09_13-58-00
site010	0.125Hz	1W	2014-09-09_11-30-00
site010	0.5Hz	1W	2014-09-09_11-46-00
site010	2Hz	1W	2014-09-09_11-51-00
site010	8Hz	1W	2014-09-09_11-54-00
site010	32Hz	1W	2014-09-09_11-56-00
site010	128Hz	1W	2014-09-09_11-58-00
site010	0.125Hz	2N	2014-09-09_11-00-00
site010	0.5Hz	2N	2014-09-09_11-16-00
site010	2Hz	2N	2014-09-09_11-21-00
site010	8Hz	2N	2014-09-09_11-24-00
site010	32Hz	2N	2014-09-09_11-26-00
site010	128Hz	2N	2014-09-09_11-28-00
site011	0.125Hz	1W	2014-09-09_14-00-00
site011	0.5Hz	1W	2014-09-09_14-16-00
site011	2Hz	1W	2014-09-09_14-21-00
site011	8Hz	1W	2014-09-09_14-24-00
site011	32Hz	1W	2014-09-09_14-26-00
site011	128Hz	1W	2014-09-09_14-28-00
site011	0.125Hz	2N	2014-09-09_13-30-00
site011	0.5Hz	2N	2014-09-09_13-46-00
site011	2Hz	2N	2014-09-09_13-51-00
site011	8Hz	2N	2014-09-09_13-54-00
site011	32Hz	2N	2014-09-09_13-56-00
site011	128Hz	2N	2014-09-09_13-58-00
site012	0.125Hz	1W	2014-09-09_14-00-00
site012	0.5Hz	1W	2014-09-09_14-16-00
site012	2Hz	1W	2014-09-09_14-21-00
site012	8Hz	1W	2014-09-09_14-24-00
site012	32Hz	1W	2014-09-09_14-26-00
site012	128Hz	1W	2014-09-09_14-28-00
site012	0.125Hz	2N	2014-09-09_14-35-00
site012	0.5Hz	2N	2014-09-09_14-51-00
site012	2Hz	2N	2014-09-09_14-56-00
site012	8Hz	2N	2014-09-09_14-59-00
site012	32Hz	2N	2014-09-09_15-01-00
site012	128Hz	2N	2014-09-09_15-03-00
site013	0.125Hz	1W	2014-09-09_11-30-00
site013	0.5Hz	1W	2014-09-09_11-46-00
site013	2Hz	1W	2014-09-09_11-51-00
site013	8Hz	1W	2014-09-09_11-54-00
site013	32Hz	1W	2014-09-09_11-56-00
site013	128Hz	1W	2014-09-09_11-58-00
site013	0.125Hz	2N	2014-09-09_11-00-00
site013	0.5Hz	2N	2014-09-09_11-16-00
site013	2Hz	2N	2014-09-09_11-21-00
site013	8Hz	2N	2014-09-09_11-24-00
site013	32Hz	2N	2014-09-09_11-26-00
site013	128Hz	2N	2014-09-09_11-28-00
site014	0.125Hz	1W	2014-09-08_10-00-00
site014	0.5Hz	1W	2014-09-08_10-16-00
site014	2Hz	1W	2014-09-08_10-21-00
site014	8Hz	1W	2014-09-08_10-24-00
site014	32Hz	1W	2014-09-08_10-26-00
site014	128Hz	1W	2014-09-08_10-28-00
site014	0.125Hz	2N	2014-09-08_10-30-00
site014	0.5Hz	2N	2014-09-08_10-46-00
site014	2Hz	2N	2014-09-08_10-51-00
site014	8Hz	2N	2014-09-08_10-54-00
site014	32Hz	2N	2014-09-08_10-56-00
site014	128Hz	2N	2014-09-08_10-58-00
site050	0.125Hz	1W	2014-09-10_14-50-00
site050	0.5Hz	1W	2014-09-10_15-06-00
site050	2Hz	1W	2014-09-10_15-42-00
site050	8Hz	1W	2014-09-10_15-45-00
site050	32Hz	1W	2014-09-10_15-47-00
site050	128Hz	1W	2014-09-10_15-49-00
site050	0.125Hz	2N	2014-09-10_14-20-00
site050	0.5Hz	2N	2014-09-10_14-36-00
site050	2Hz	2N	2014-09-10_14-41-00
site050	8Hz	2N	2014-09-10_14-44-00
site050	32Hz	2N	2014-09-10_14-46-00
site050	128Hz	2N	2014-09-10_14-48-00
site051	0.125Hz	1W	2014-09-10_14-50-00
site051	0.5Hz	1W	2014-09-10_15-06-00
site051	2Hz	1W	2014-09-10_15-11-00
site051	8Hz	1W	2014-09-10_15-14-00
site051	32Hz	1W	2014-09-10_15-16-00
site051	128Hz	1W	2014-09-10_15-18-00
site051	0.125Hz	2N	2014-09-10_14-20-00
site051	0.5Hz	2N	2014-09-10_14-36-00
site051	2Hz	2N	2014-09-10_14-41-00
site051	8Hz	2N	2014-09-10_14-44-00
site051	32Hz	2N	2014-09-10_14-46-00
site051	128Hz	2N	2014-09-10_14-48-00
site080	0.125Hz	1W	2014-09-10_14-50-00
site080	0.5Hz	1W	2014-09-10_15-06-00
site080	2Hz	1W	2014-09-10_15-11-00
site080	8Hz	1W	2014-09-10_15-14-00
site080	32Hz	1W	2014-09-10_15-16-00
site080	128Hz	1W	2014-09-10_15-18-00
site080	0.125Hz	2N	2014-09-10_14-20-00
site080	0.5Hz	2N	2014-09-10_14-36-00
site080	2Hz	2N	2014-09-10_14-41-00
site080	8Hz	2N	2014-09-10_14-44-00
site080	32Hz	2N	2014-09-10_14-46-00
site080	128Hz	2N	2014-09-10_14-48-00
site101	2Hz	1W	2014-09-10_09-21-00
site101	8Hz	1W	2014-09-10_09-24-00
site101	32Hz	1W	2014-09-10_09-26-00
site101	128Hz	1W	2014-09-10_09-28-00
site101	0.125Hz	1W	2014-09-10_09-45-00
site101	0.5Hz	1W	2014-09-10_10-01-00
site101	0.125Hz	2N	2014-09-10_08-30-00
site101	0.5Hz	2N	2014-09-10_08-46-00
site101	2Hz	2N	2014-09-10_08-51-00
site101	8Hz	2N	2014-09-10_08-54-00
site101	32Hz	2N	2014-09-10_08-56-00
site101	128Hz	2N	2014-09-10_08-58-00
site102	0.125Hz	1W	2014-09-10_11-45-00
site102	0.5Hz	1W	2014-09-10_12-01-00
site102	2Hz	1W	2014-09-10_12-06-00
site102	8Hz	1W	2014-09-10_12-09-00
site102	32Hz	1W	2014-09-10_12-11-00
site102	128Hz	1W	2014-09-10_12-13-00
site102	0.125Hz	2N	2014-09-10_11-15-00
site102	0.5Hz	2N	2014-09-10_11-31-00
site102	2Hz	2N	2014-09-10_11-36-00
site102	8Hz	2N	2014-09-10_11-39-00
site102	32Hz	2N	2014-09-10_11-41-00
site102	128Hz	2N	2014-09-10_11-43-00
site103	2Hz	1W	2014-09-10_09-21-00
site103	8Hz	1W	2014-09-10_09-24-00
site103	32Hz	1W	2014-09-10_09-26-00
site103	128Hz	1W	2014-09-10_09-28-00
site103	0.125Hz	1W	2014-09-10_09-45-00
site103	0.5Hz	1W	2014-09-10_10-01-00
site103	0.125Hz	2N	2014-09-10_08-30-00
site103	0.5Hz	2N	2014-09-10_08-46-00
site103	2Hz	2N	2014-09-10_08-51-00
site103	8Hz	2N	2014-09-10_08-54-00
site103	32Hz	2N	2014-09-10_08-56-00
site103	128Hz	2N	2014-09-10_08-58-00
site104	0.125Hz	1W	2014-09-10_11-45-00
site104	0.5Hz	1W	2014-09-10_12-01-00
site104	2Hz	1W	2014-09-10_12-06-00
site104	8Hz	1W	2014-09-10_12-09-00
site104	32Hz	1W	2014-09-10_12-11-00
site104	128Hz	1W	2014-09-10_12-13-00
site104	0.125Hz	2N	2014-09-10_11-15-00
site104	0.5Hz	2N	2014-09-10_11-31-00
site104	2Hz	2N	2014-09-10_11-36-00
site104	8Hz	2N	2014-09-10_11-39-00
site104	32Hz	2N	2014-09-10_11-41-00
site104	128Hz	2N	2014-09-10_11-43-00
site105	0.125Hz	1W	2014-09-10_11-45-00
site105	0.5Hz	1W	2014-09-10_12-01-00
site105	2Hz	1W	2014-09-10_12-06-00
site105	8Hz	1W	2014-09-10_12-09-00
site105	32Hz	1W	2014-09-10_12-11-00
site105	128Hz	1W	2014-09-10_12-13-00
site105	0.125Hz	2N	2014-09-10_11-15-00
site105	0.5Hz	2N	2014-09-10_11-31-00
site105	2Hz	2N	2014-09-10_11-36-00
site105	8Hz	2N	2014-09-10_11-39-00
site105	32Hz	2N	2014-09-10_11-41-00
site105	128Hz	2N	2014-09-10_11-43-00
site106	0.125Hz	1W	2014-09-10_07-45-00
site106	0.5Hz	1W	2014-09-10_08-01-00
site106	2Hz	1W	2014-09-10_08-06-00
site106	8Hz	1W	2014-09-10_08-09-00
site106	32Hz	1W	2014-09-10_08-11-00
site106	128Hz	1W	2014-09-10_08-13-00
site106	0.125Hz	2N	2014-09-10_07-15-00
site106	0.5Hz	2N	2014-09-10_07-31-00
site106	2Hz	2N	2014-09-10_07-36-00
site106	8Hz	2N	2014-09-10_07-39-00
site106	32Hz	2N	2014-09-10_07-41-00
site106	128Hz	2N	2014-09-10_07-43-00
site107	2Hz	1W	2014-09-06_14-21-00
site107	8Hz	1W	2014-09-06_14-24-00
site107	32Hz	1W	2014-09-06_14-26-00
site107	128Hz	1W	2014-09-06_14-28-00
site107	0.125Hz	1W	2014-09-06_15-15-00
site107	0.5Hz	1W	2014-09-06_15-31-00
site107	0.125Hz	2N	2014-09-06_14-30-00
site107	0.5Hz	2N	2014-09-06_14-46-00
site107	2Hz	2N	2014-09-06_14-51-00
site107	8Hz	2N	2014-09-06_14-54-00
site107	32Hz	2N	2014-09-06_14-56-00
site107	128Hz	2N	2014-09-06_14-58-00
site107	0.125Hz	1W	2014-09-08_07-00-00
site107	0.5Hz	1W	2014-09-08_07-16-00
site107	2Hz	1W	2014-09-08_07-21-00
site107	8Hz	1W	2014-09-08_07-24-00
site107	32Hz	1W	2014-09-08_07-26-00
site107	128Hz	1W	2014-09-08_07-28-00
site107	0.125Hz	2N	2014-09-08_10-30-00
site107	0.5Hz	2N	2014-09-08_10-46-00
site107	2Hz	2N	2014-09-08_10-51-00
site107	8Hz	2N	2014-09-08_10-54-00
site107	32Hz	2N	2014-09-08_10-56-00
site108	0.125Hz	1W	2014-09-08_09-00-00
site108	0.5Hz	1W	2014-09-08_09-16-00
site108	2Hz	1W	2014-09-08_09-21-00
site108	8Hz	1W	2014-09-08_09-24-00
site108	32Hz	1W	2014-09-08_09-26-00
site108	128Hz	1W	2014-09-08_09-28-00
site108	0.125Hz	2N	2014-09-08_09-30-00
site108	0.5Hz	2N	2014-09-08_09-46-00
site108	2Hz	2N	2014-09-08_09-51-00
site108	8Hz	2N	2014-09-08_09-54-00
site108	32Hz	2N	2014-09-08_09-56-00
site108	128Hz	2N	2014-09-08_09-58-00
site109	0.125Hz	1W	2014-09-08_07-00-00
site109	0.5Hz	1W	2014-09-08_07-16-00
site109	2Hz	1W	2014-09-08_07-21-00
site109	8Hz	1W	2014-09-08_07-24-00
site109	32Hz	1W	2014-09-08_07-26-00
site109	128Hz	1W	2014-09-08_07-28-00
site109	0.125Hz	2N	2014-09-08_09-30-00
site109	0.5Hz	2N	2014-09-08_09-46-00
site109	0.125Hz	2N	2014-09-08_10-30-00
site109	0.5Hz	2N	2014-09-08_10-46-00
site110	0.125Hz	1W	2014-09-06_14-00-00
site110	0.5Hz	1W	2014-09-06_14-16-00
site110	2Hz	1W	2014-09-06_14-21-00
site110	8Hz	1W	2014-09-06_14-24-00
site110	32Hz	1W	2014-09-06_14-26-00
site110	128Hz	1W	2014-09-06_14-28-00
site110	0.125Hz	2N	2014-09-06_14-30-00
site110	0.5Hz	2N	2014-09-06_14-46-00
site110	2Hz	2N	2014-09-06_14-51-00
site110	8Hz	2N	2014-09-06_14-54-00
site110	32Hz	2N	2014-09-06_14-56-00
site110	128Hz	2N	2014-09-06_14-58-00
site110	0.125Hz	1W	2014-09-08_08-50-00
site110	0.5Hz	1W	2014-09-09_09-06-00
site110	2Hz	1W	2014-09-09_09-11-00
site110	8Hz	1W	2014-09-09_09-14-00
site110	32Hz	1W	2014-09-09_09-16-00
site110	128Hz	1W	2014-09-09_09-18-00
site110	0.125Hz	2N	2014-09-09_08-20-00
site110	0.5Hz	2N	2014-09-09_08-36-00
site110	2Hz	2N	2014-09-09_08-41-00
site110	8Hz	2N	2014-09-09_08-44-00
site110	32Hz	2N	2014-09-09_08-46-00
site110	128Hz	2N	2014-09-09_08-48-00
site111	0.125Hz	1W	2014-09-10_07-45-00
site111	0.5Hz	1W	2014-09-10_08-01-00
site111	2Hz	1W	2014-09-10_08-06-00
site111	8Hz	1W	2014-09-10_08-09-00
site111	32Hz	1W	2014-09-10_08-11-00
site111	128Hz	1W	2014-09-10_08-13-00
site111	0.125Hz	2N	2014-09-10_07-15-00
site111	0.5Hz	2N	2014-09-10_07-31-00
site111	2Hz	2N	2014-09-10_07-36-00
site111	8Hz	2N	2014-09-10_07-39-00
site111	32Hz	2N	2014-09-10_07-41-00
site111	128Hz	2N	2014-09-10_07-43-00
site112	0.125Hz	1W	2014-09-10_07-45-00
site112	0.5Hz	1W	2014-09-10_08-01-00
site112	2Hz	1W	2014-09-10_08-06-00
site112	8Hz	1W	2014-09-10_08-09-00
site112	32Hz	1W	2014-09-10_08-11-00
site112	128Hz	1W	2014-09-10_08-13-00
site112	0.125Hz	2N	2014-09-10_07-15-00
site112	0.5Hz	2N	2014-09-10_07-31-00
site112	2Hz	2N	2014-09-10_07-36-00
site112	8Hz	2N	2014-09-10_07-39-00
site112	32Hz	2N	2014-09-10_07-41-00
site112	128Hz	2N	2014-09-10_07-43-00

Table *3*: Data acquired per station (transmitter frequency and dipole direction)

3.3 Data Processing

Data have been processed using BRGM proprietary software PROCATS (Bourgeois et al. (2012)). Transfer function between the recorded signals *(E$_x$(f), E$_y$(f), H$_x$(f), H$_y$(f))* and the transmitted signals *I(f)* are estimated in the Fourier domain for each fundamental frequency and harmonics. The obtained complex transfer functions represent the electric and magnetic earth response to a unitary current injection (in mV/m/A and mA/m/A, Figure 21). Noise levels are also estimated and will be later used to exclude some data from the interpretation.
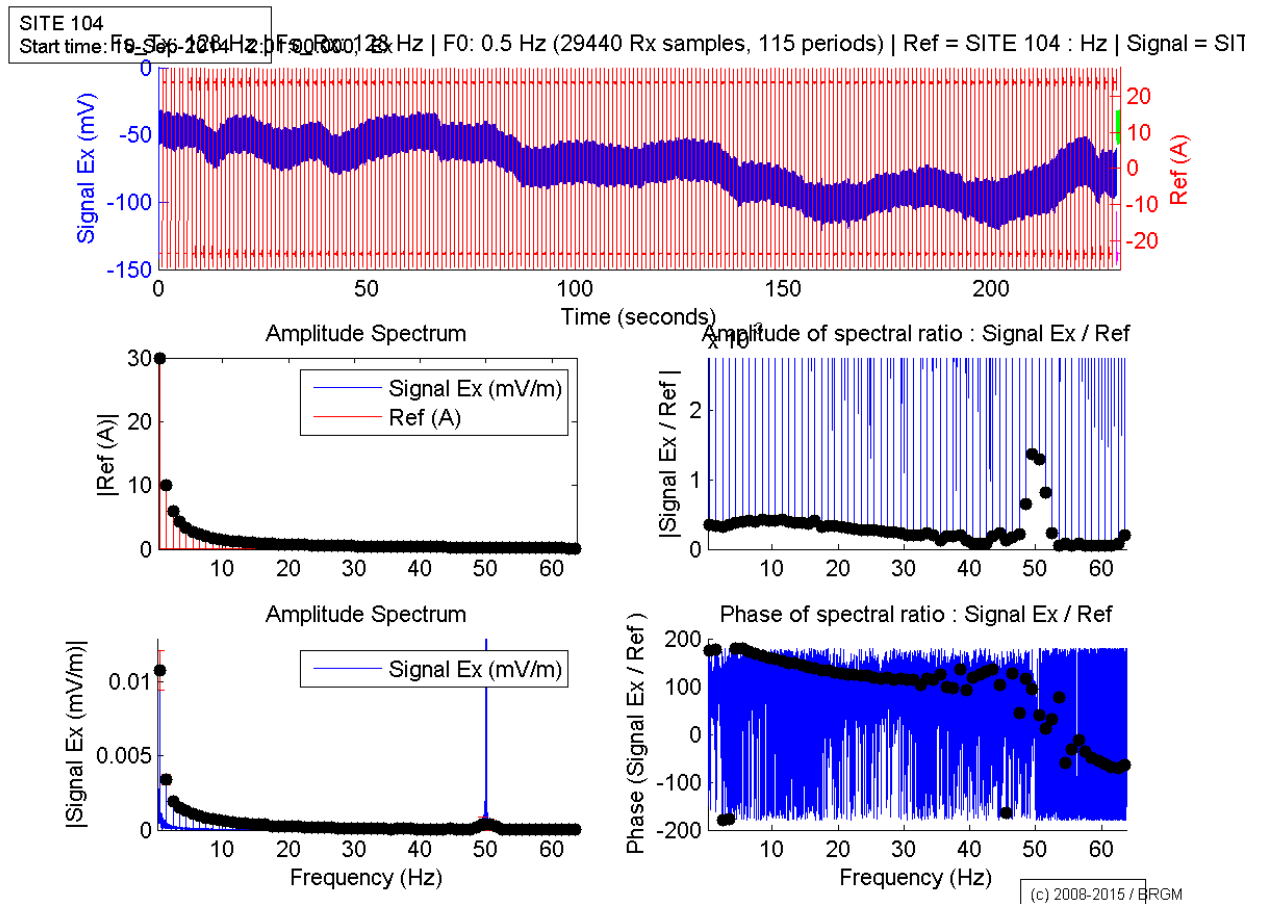
Figure 21 : Processing QC plots for station 104, polarisation 1, fondamental frequency 0.5 Hz. Top : time series of the transmitted current (red) and recorded electric signal along Ex (blue). Middle-left: amplitude spectrum of the trasmitted signal. Bottom-left: same for the recorded electric field. Middle right: amplitude ratio between electric field and injected current. Bottom right: phase difference between the electric field and injected current.

3.4 Results

3.4.1 Data quality and influence of cultural noise

A high level of cultural noise is expected in the area of interest due to the proximity of the Litomerice city and industrial activities. A typical example of noise is shown on Figure 22 where we can observe a well pronounced peak of energy at 50Hz and its harmonics caused by power lines. For this particular recording station located in the middle of the city, this noise is as strong as the CSEM signal transmitted at the fundamental frequency of 128 Hz and polarization 1 (black dot at 128 Hz at the bottom left of the figure) making the CSEM signal unusable. It is however interesting to realize that the noise is very polarized at this station making the Ey component roughly four times more noisy than the Ex component (Figure 23). As a consequence, transmitting a CSEM signal polarized differently (e.g. polarization 2) allows recording a reliable CSEM signal on the Ex component of this station (signal/noise ratio greater than 10, see Figure 24). This emphasizes the effectiveness of acquiring two different types of source polarization during CSEM surveys.

For some recording stations, the noise levels are acceptable over the frequency band of interest but still some monochromatic noises are present (Figure 25). Such noises are easily filtered out in the frequency domain and therefore do not pose any serious issues.
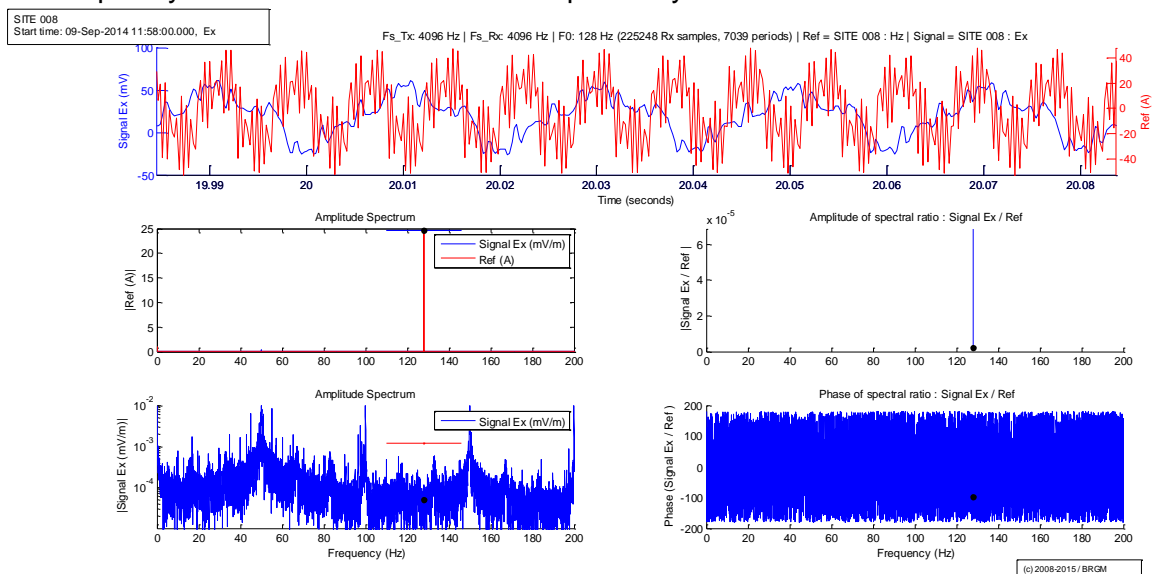
Figure 22 : Processing QC plots for station 008, polarisation 1, fundamental frequency 128Hz. Top: time series of the transmitted current (red) and recorded electric signal along Ex (blue). Middle-left: amplitude spectrum of the transmitted signal. Bottom-left: same for the recorded electric field. Middle right: amplitude ratio between electric field and injected current. Bottom right: phase difference between the electric field and injected current

Given the diversity of noises present in the dataset, we used frequency domain noise level estimates, Argand diagrams, polarization ellipses as well as a visual inspection of the amplitude spectra to accept or reject the electric fields recorded at all stations and frequencies of interest. Results are summarized on Table 4. Excluding stations 080, 050 and 051 which are not in the area of interest, it is very satisfactory to observe that we have no data gap despite the presence of high level of cultural noise. This demonstrates that a CSEM acquisition is very efficient way of acquiring good quality EM soundings in noisy areas.

To establish the feasibility of future CSEM surveys in noisy environment, we have summarized on Table 5 the typical noise levels observed on the electric fields at the different frequency bands (assuming the same recording lengths per frequency as during the Litomerice survey).
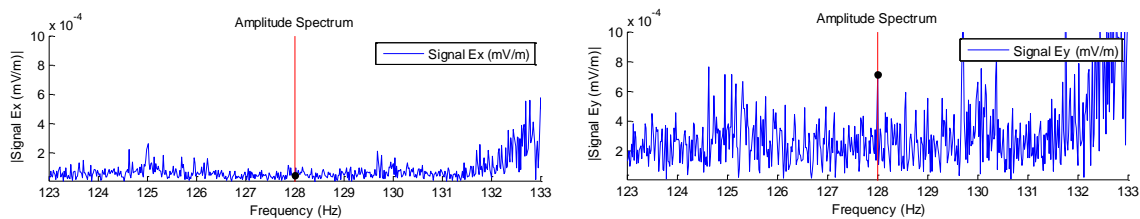
Figure 23 : Amplitude spectrum of the Ex (left) and Ey (right) components of the station 008 during the source transmission of polarisation 1 and fundamental frequency 128Hz.
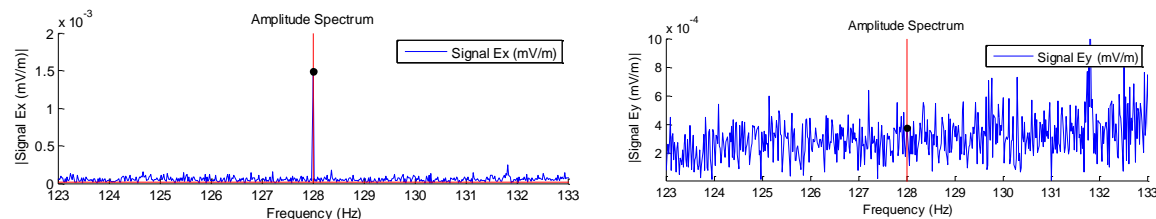
Figure 24 : Amplitude spectrum of the Ex (left) and Ey (right) components of the station 008 during the source transmission of polarisation 2 and fundamental frequency 128Hz.
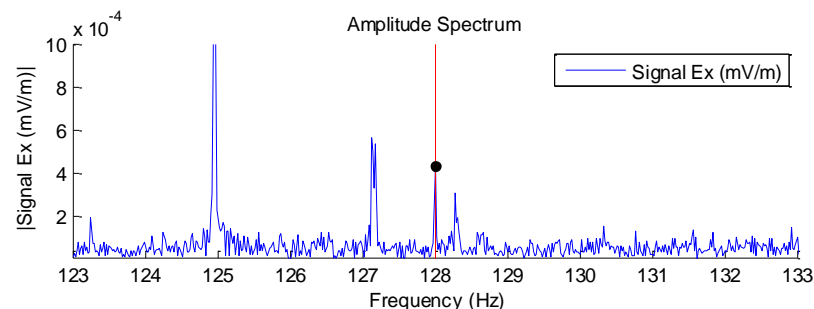
Figure 25 : Amplitude spectrum of the Ex (left) components of the station 006 during the source transmission of polarisation 1 and fundamental frequency 128Hz.

0.125Hz (top left)

	POL1				POL2		
Station	NoiseEx/Ex(%)	NoiseEy/Ey(%)	KEEP?	Station2	NoiseEx/Ex(%)3	NoiseEy/Ey(%)4	KEEP?5
site001	0.575663967	0.358930744	Yes	site001	3.869837354	2.978986625	Yes
site003	0.761062457	0.852776519	Yes	site003	0.675225426	1.030448625	Yes
site004	6.115883811	5.297856615	Yes	site004	4.288048867	6.171649537	Yes
site005	12.82683291	5.372314025	Yes	site005	4.966832934	10.58002665	Yes
site006	3.374811347	8.16431837	Yes	site006	4.069057177	25.0070268	Yes
site007	5.291612985	12.94327819	Yes	site007	5.392897761	15.67170872	Yes
site008	10.20740375	9.865538884	Yes	site008	17.50331802	21.10295607	Yes
site009	5.900750778	15.19375904	Yes	site009	7.059701763	16.915871	Yes
site010	13.20136731	254.6216766	Yes	site010	20.23040868	186.8067148	Yes
site011	8.119638612	9.776601109	Yes	site011	17.58781507	18.44239717	Yes
site012	3.689120462	1.574397029	Yes	site012	5.830816876	3.156098293	Yes
site013	3.352315246	1.944697082	Yes	site013	4.040236872	3.217405789	Yes
site014	16.89164584	13.97729127	Yes	site014	12.01784718	18.50239269	Yes
site050	122.6697263	114.9393153	No	site050	238.4960635	469.605784	No
site051	82.23317167	68.61600464	Yes	site051	56.69296792	66.54255931	No
site080	165.5301598	90.11914668	No	site080	118.7801149	89.88303238	No
site101	0.56652217	0.597883283	Yes	site101	0.657958596	1.341260849	Yes
site102	6.131809626	1.166492961	Yes	site102	2.061524039	2.810956662	Yes
site103	1.513262952	0.914145701	Yes	site103	3.246511783	6.581435796	Yes
site104	13.10432257	1.555414053	Yes	site104	9.37001531	6.680201097	Yes
site105	33.90324921	2.450409128	Yes	site105	19.94916263	8.085787119	Yes
site106	92.72068845	15.22577723	No	site106	8.650419048	1.222817247	Yes
site107	5.709902082	24.00720027	Yes	site107	2.530460512	1.479802766	Yes
site107	22.9597726	99.44734846	Yes	site107	2.655383943	0.894279547	Yes
site108	11.09500723	23.88673954	Yes	site108	3.208151237	3.804852559	Yes
site109	10.21475998	20.21616795	Yes	site109	7.028247625	2.396821731	Yes
				site109	4.261450055	3.681635059	Yes
site110	13.06540641	21.19366165	Yes	site110	21.16780776	7.844923795	Yes
site110	5.020275439	28.25464358	Yes	site110	15.85426327	9.487078102	Yes
site111	8.744261755	7.091560736	Yes	site111	41.38164727	5.42986645	Yes
site112	24.99949172	28.50873302	Yes	site112	1.660389722	4.126632566	Yes

8Hz (top right)

	POL1				POL2		
Station	NoiseEx/Ex(%)	NoiseEy/Ey(%)	KEEP?	Station2	NoiseEx/Ex(%)3	NoiseEy/Ey(%)4	KEEP?5
site001	0.179589593	0.109442849	YES	site001	0.299060408	0.234032099	YES
site003	0.116098048	0.097759258	YES	site003	0.041715265	0.098794051	YES
site004	0.513982414	0.578563245	YES	site004	0.252983546	0.479369859	YES
site005	0.353273734	0.548254925	YES	site005	0.205812533	0.311523607	YES
site006	0.421024616	0.58779095	YES	site006	0.197749167	0.486246384	YES
site007	1.011355447	3.029906118	YES	site007	0.386377181	3.180474659	YES
site008	1.909271366	1.772219704	YES	site008	1.849519146	3.678297227	YES
site009	0.891908963	1.952612218	YES	site009	0.603489377	0.915110161	YES
site010	1.033120451	22.17597388	YES	site010	0.98502038	11.46714367	YES
site011	0.95225939	1.209937986	YES	site011	0.668049626	0.892158603	YES
site012	0.52209256	0.260915973	YES	site012	1.116429115	0.364343317	YES
site013	0.262888212	0.170566093	YES	site013	0.204721446	0.171040488	YES
site014	2.398418309	2.178086381	YES	site014	3.151346044	4.264488584	YES
site050	29.65272174	10.71172092	YES	site050	137.3687606	15.27251534	YES
site051	31.4820432	41.21982938	YES	site051	13.26959567	23.06483267	YES
site080	145.7764337	123.2289346	No	site080	51.94794037	153.4435474	No
site101	0.191105791	0.098865635	YES	site101	0.070689768	0.093537004	YES
site102	0.318407679	0.057357089	YES	site102	0.208043933	0.166067996	YES
site103	1.141750995	0.282000895	YES	site103	0.318169065	0.403728754	YES
site104	0.486040458	0.145288116	YES	site104	1.762628605	0.629004308	YES
site105	1.594641733	0.213674987	YES	site105	3.923070433	0.64056524	YES
site106	1.776422385	1.477388886	YES	site106	0.644405185	0.131997363	YES
site107	0.328353992	2.348739097	YES	site107	0.353442135	0.065365859	YES
site107	0.495849278	0.964822441	YES	site107	0.217102495	0.160553628	YES
site108	0.970666513	2.675864447	YES	site108	0.186148882	0.415111642	YES
site109	1.055648062	2.395159039	YES				
site110	1.51979441	2.397659222	YES	site110	4.83159223	0.978391081	YES
site110	0.822954713	1.181259509	YES	site110	4.87269292	1.161242736	YES
site111	1.246800652	0.870129408	YES	site111	21.57476548	0.693531609	YES
site112	3.192838015	6.63611639	YES	site112	0.107025151	0.537605205	YES

32Hz (bottom left)

Station	NoiseEx/Ex(%)	NoiseEy/Ey(%)	KEEP?	Station2	NoiseEx/Ex(%)3	NoiseEy/Ey(%)4	KEEP?5
site001	0.204182559	0.127944957	YES	site005	0.375106934	1.49079753	YES
site003	0.208371611	0.250904403	YES	site006	0.63650708	2.216099907	YES
site004	1.902489738	2.453631321	YES	site007	1.983356202	14.00064155	YES
site006	0.956043976	4.082907674	YES	site008	9.174649977	40.33052932	YES
site007	2.373278356	10.34302498	YES	site009	29.1446989	9.113688325	YES
site008	22.99272482	29.3290354	YES	site010	9.194963619	74.6328664	YES
site009	16.49058105	7.317244498	YES	site011	3.638780038	15.72780259	YES
site010	7.476044619	86.1411782	YES	site012	1.245346063	0.905140211	YES
site011	5.893157384	13.11178596	YES	site013	0.763945787	0.326348177	YES
site012	1.698088282	1.591320839	YES	site014	22.09328942	15.88391193	YES
site013	0.407761695	0.254383953	YES	site050	39.24433978	13.12268406	YES
site014	21.83937348	14.76722426	YES	site051	18.9319175	73.86606323	YES
site050	11.24425119	7.876219859	YES	site080	89.31880643	88.60092088	No
site051	21.58109134	77.61023566	YES	site101	0.070936076	0.108253796	YES
site080	238.8615307	92.69414598	No	site102	0.072128583	0.105862617	YES
site101	0.057180304	0.109983139	YES	site103	0.668114925	0.409178273	YES
site102	0.762574707	0.108127924	YES	site104	1.194979776	0.590058486	YES
site103	0.366568131	0.383782261	YES	site105	8.954778517	0.94331132	YES
site104	1.096542799	0.502209247	YES	site106	0.124448945	0.066349472	YES
site105	11.55579083	0.773239843	YES	site107	0.065207772	0.193498892	YES
site106	0.490081186	1.110116907	YES	site107	0.038481192	0.049678805	YES
site107	0.090371582	0.251631368	YES	site108	0.149752336	2.20460501	YES
site107	0.13311147	0.474775636	YES	site110	1.53305319	6.475072134	YES
site108	1.236944018	0.57298411	YES	site110	1.607333084	6.411086541	YES
site109	2.365711324	5.741443214	YES	site111	3.031190735	4.948042289	YES
site110	2.19867637	12.95922865	YES	site112	0.054887108	0.403011342	YES
site110	1.762453326	14.41205716	YES				
site111	3.832299469	5.892678666	YES				
site112	0.979812748	2.031452256	YES				

128Hz (bottom right)

Station	NoiseEx/Ex(%)	NoiseEy/Ey(%)	KEEP?	Station2	NoiseEx/Ex(%)3	NoiseEy/Ey(%)4	KEEP?5
site001	2.771472382	0.595848078	Yes	site001	16.78208415	1.289183179	Yes
site003	0.866090683	2.062099323	Yes	site003	0.214827281	0.665420342	Yes
site004	13.8233863	47.82954311	Yes	site004	12.39384437	45.62648744	Yes
site005	6.205296983	17.84764901	Yes	site005	10.61147505	101.7331166	Yes
site006	538.6588559	501.3815567	Yes	site006	24.65656355	106.2102619	Yes
site007	331.8480914	1639.653937	Yes	site007	363.7012325	148.3025853	Yes
site008	2358.269473	1972.538891	No	site008	99.10127067	3887.13694	Yes
site009	190.7050318	45.82319633	No	site009	72.94365398	189.8875159	Yes
site010	221.2698691	24074.82179	Yes	site010	400.8298415	257.7712584	Yes
site011	25.88422195	84.81505961	Yes	site011	11.61518265	33.7428538	Yes
site012	14.22224646	23.7499003	Yes	site012	19.83298072	3.997288271	Yes
site013	16.78523868	5.684917652	Yes	site013	5.804790203	1.033775853	Yes
site014	4915.701073	12759.87571	No	site014	673.9395857	517.2746511	Yes
site050	112.920448	45.39110353	Yes	site050	145.5270791	55.2960021	Yes
site051	105.1740695	1144.064341	Yes	site051	68.86732341	99.43329206	Yes
site080	271.4300091	397.2300433	No	site080	124.4026991	2597.848794	No
site101	0.115370559	0.454214372	Yes	site101	0.049984403	0.114194259	Yes
site102	3.729493698	1.68423185	Yes	site102	1.016585943	0.727488148	Yes
site103	6.108821514	2.165702484	Yes	site103	4.490364381	2.268038203	Yes
site104	3.49391753	1.323913964	Yes	site104	3.130988762	0.497062286	Yes
site105	12.82649362	6.885197482	Yes	site105	2.567918606	5.12523717	Yes
site106	0.174310475	1.278436825	Yes	site106	0.230974843	0.125251077	Yes
site107	0.597059349	1.233745922	Yes	site107	0.075320671	0.088985737	Yes
site107	0.06537589	1.003763404	Yes				
site108	1.133188449	0.958639611	Yes	site108	1.26358954	0.772759369	Yes
site109	5.799077353	5.541516236	Yes				
site110	16.62866417	23.09131427	Yes	site110	5.806544133	18.41685688	Yes
site110	20.20568705	27.85763307	Yes	site110	3.365739767	10.07563624	Yes
site111	38.58494996	20.88974556	Yes	site111	9.80923008	24.47265471	Yes
site112	0.560766426	1.004779639	Yes	site112	0.158574786	1.637979543	Yes

Table 4 : Summary table of all recorded signals for the two types of source polarizations and fundamental frequencies of 0.125Hz (top left), 8Hz (top right), 32Hz (bottom left) and 128Hz (bottom right).

Frequency	Quiet	Noisy	Very Noisy
0.125Hz	10^{-11} V/A.m^2	10^{-10} V/A.m^2	Not observed
0.5Hz	10^{-12} V/A.m^2	10^{-11} V/A.m^2	Not observed
2Hz	10^{-12} V/A.m^2	10^{-11} V/A.m^2	Not observed
8Hz	10^{-12} V/A.m^2	10^{-11} V/A.m^2	Not observed
32Hz	10^{-12} V/A.m^2	10^{-11} V/A.m^2	Not observed
128Hz	10^{-12} V/A.m^2	10^{-11} V/A.m^2	10^{-10} V/A.m^2

Table 5 : Summary table of typical noise levels observed on the electric fields during the Litomerice survey. "Quiet" refers to a site away from any cultural noise (a few kilometers). "Noisy" refers to a site located in the vicinity or within a city. "Very noisy" refers to a site within a city with pronounced cultural noise. It is striking to observe despite the 128Hz, no sites located within the Litomerice city are no usable CSEM data and be classified as "very noisy".

3.4.2 1D modelling results

3.4.2.1 LEMAM setup

The source used during the CSEM survey is a LEMAM injection setup (Longue Electrode Mise à la Masse, Bourgeois and Girard (2010)). The principle of this setup is to use the metallic casing of

borehole as a long electrode for current injection. The deep geothermal exploration well PVGT-LT1 cased down to 1800 m below surface has been used as injection point (Figure 26).

Due to casing imperfections and variable background resistivities, it is difficult to predict where and how much current is flowing from the metallic casing into the formation. We therefore used a data-driven approach to establish an equivalent length of the energized casing. Figure 27 shows modelled and observed polarization ellipses at 0.5 Hz for different modelled length of energized casing. We used a 3D modelling code developed at the BRGM to simulate the different responses. Since the effect of the casing length is the strongest near the source (Kong et al. 2009), we only compared the polarization ellipses of the stations closest to the borehole (Figure 27). The best match is obtained for the short vertical wire of 200 m. This is explained by the fact that most of the injected current goes into the formation within the first few hundreds of meters, where the most conductive formation (recent sediments from Cretaceous and Quaternary) can be found (Figure 28).
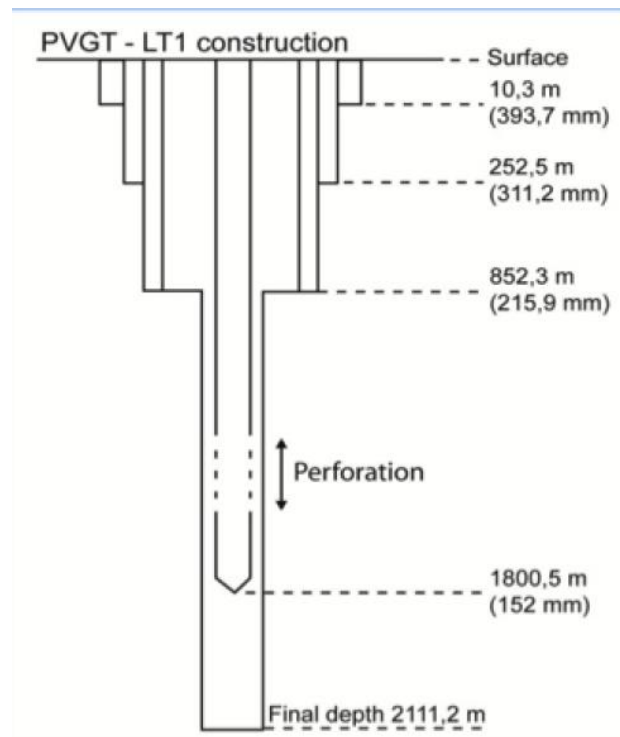
Figure 26 : Deep geothermal exploration well PVGT-LT1 cased down to 1800m below surface used as injection point for the LEMAM setup.
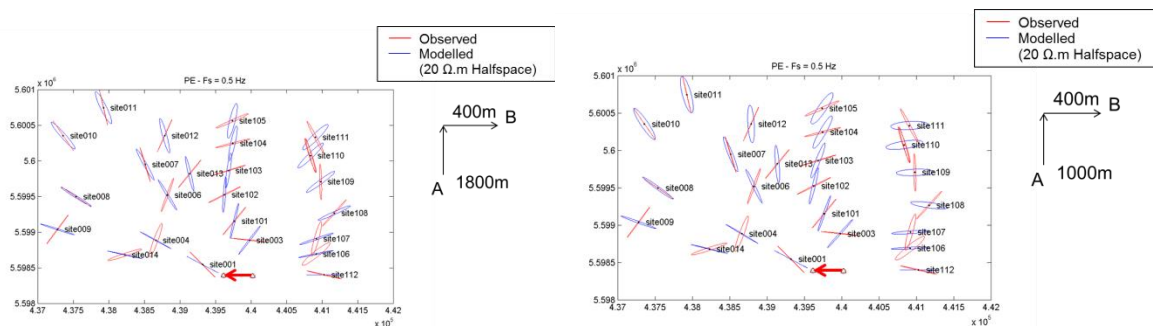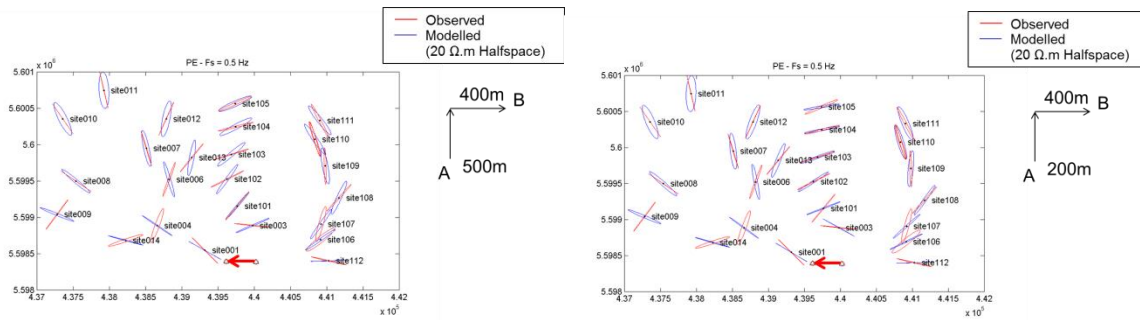
**Figure 27 : Map view of the modelled and observed polarization ellipses at 0.5Hz for different modelled length of energized casing (top left: 400m long horizontal wire + 1800m long vertical wire, top right: 400m long horizontal wire + 1000m long vertical wire, bottom left: 400m long horizontal wire + 500m long vertical wire, bottom right: 400m long horizontal wire + 200m long vertical wire).**
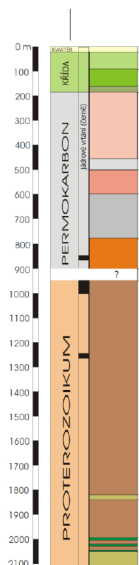
Geology & stratigraphy, PVGT-LT1

0 - 25 m	Quaternary	
25 - 165 m	Cretaceous - Turonian	
165 - 190 m	Cretaceous - Cenomanian	
190 - 780 m	Permo-Carboniferous	190 - 460 m Líně Fm.
		460 - 500 m Slaný Fm.
		500 - 600 m Týnec Fm.
		600 - 780 m Kladno Fm.
780 - 910 m	"Teplice porphyry"	Rhyolitic ignimbrite
910 - 942 m	?	base of Permo-Carboniferous unit
942 - 2050 m	Proterozoic crystalline basement	mica schist with interlayers of phyllite and actinolite-rich rock
2050 - 2110 m	Proterozoic crystalline basement	phyllite

Figure 28 : Lithological and stratigraphical description of GTPV LT-1.

3.4.2.2 1D modelling results

Figure 29 shows the modelled major axis of the polarization ellipse of the electric field generated by a 500m-long and 200m-deep vertical wire at 0.125Hz for polarization 1 embedded in a 20 Ω.m half-space to compare with the measured major axis of the polarization ellipse of the electric field at 0.125Hz for polarization 1. To take out the imprint of the field decay with the distance from the source, we computed the ratio of the two (Figure 30). It is clear that in the north-western corner of the survey a more resistive structure is present as the observed field is a lot stronger than the modelled response (more than 40 times). However, to get a feel for the spatial extent of this anomaly, the illumination pattern of the source has to be taken into account. Figure 30 shows the ratio of the modelled electric field between a 20 Ω.m half-space and a 1000 Ω.m half-space with the first 200m at 20 Ω.m, simulating the anomaly generated by a resistive basement at 1000 Ω.m at 200m depth. It shows that the sensitivity to a resistive basement is not homogeneous but increases with the distance to the source. It also shows that the sensitivity is poor near the source (roughly the first 2km). We can therefore conclude that the measured anomaly in North-Western corner is likely to be caused by a resistive body at depth (most likely the basement) while the absence of an anomaly in the North-Eastern corner is likely to be caused by a deeper basement. However, the absence of an anomaly in the South-Eastern corner may be caused either by the absence of resistive basement or simply by the poor sensitivity of the CSEM survey near the

source. To resolve this ambiguity, a second source would have to be deployed in the northern side of the survey to balance the source imprint.
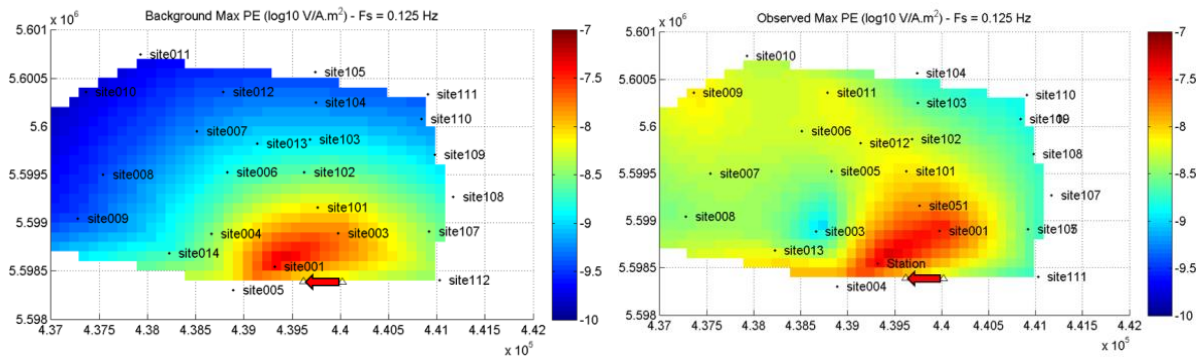

Figure 29 : Left: Map view of the modelled major axis of the polarization ellipse of the electric field generated by a 500m-long and 200m-deep vertical wire at 0.125Hz for polarization 1 embedded in a 20 Ω.m half-space. Right: Map view of the observed major axis of the polarization ellipse of the electric field at 0.125Hz for polarization 1.
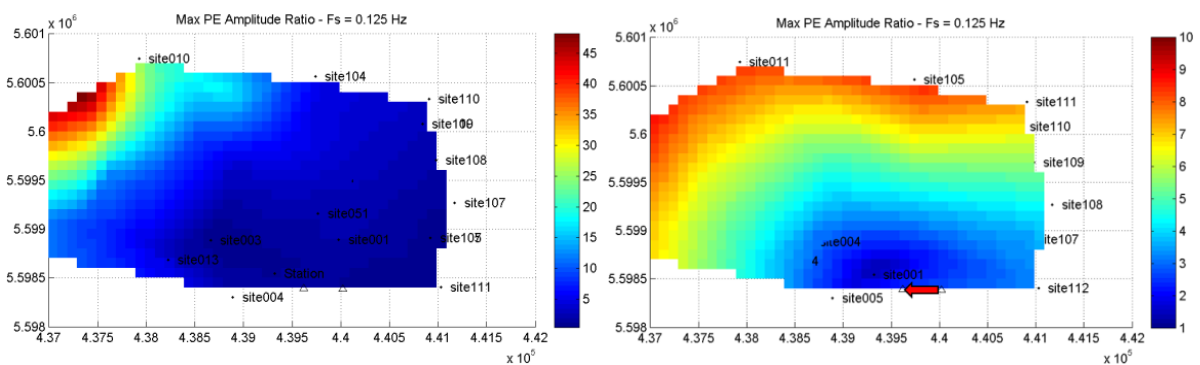

Figure 30 : Map view of the ratio of the measured (left) and modelled (right) major axis of the polarization ellipse of the electric field at 0.125Hz for polarization 1.

In order to visualize the CSEM anomalies observed in the dataset, we have computed for every station, every source fundamental frequency and polarization an equivalent half-space resistivity model. To do so, we have searched for the best match between the modelled and measured maximum axis of the polarization ellipses of the electric fields (Figure 31). Figure 32 and Figure 33show the obtained half-space resistivity map after interpolation between every station for polarization 1 and 2, respectively. Results are very consistent for both polarizations and from one frequency to next, highlighting the robustness of the measured CSEM signals. We can observe on the lowest frequencies (0.125, 0.625, 2.125 and 8Hz) that a very resistive body (around 1000 Ω.m) is present in the North-Western corner of the survey and becomes abruptly less resistive to the North-East (less than 100 Ω.m). This resistive body is likely to be deep (> 500m) as the lowest frequencies have the deepest depth of penetration (Figure 34). On the contrary, the highest frequencies (32 and 128 Hz) do no exhibit any significant resistive anomalies and suggest a rather laterally homogenous shallow conductive layer (~20 Ω.m at less 500m depth). Finally, the highest frequency (128 Hz) shows locally some conductive anomalies (a few Ω.m) underneath Litomerice city.
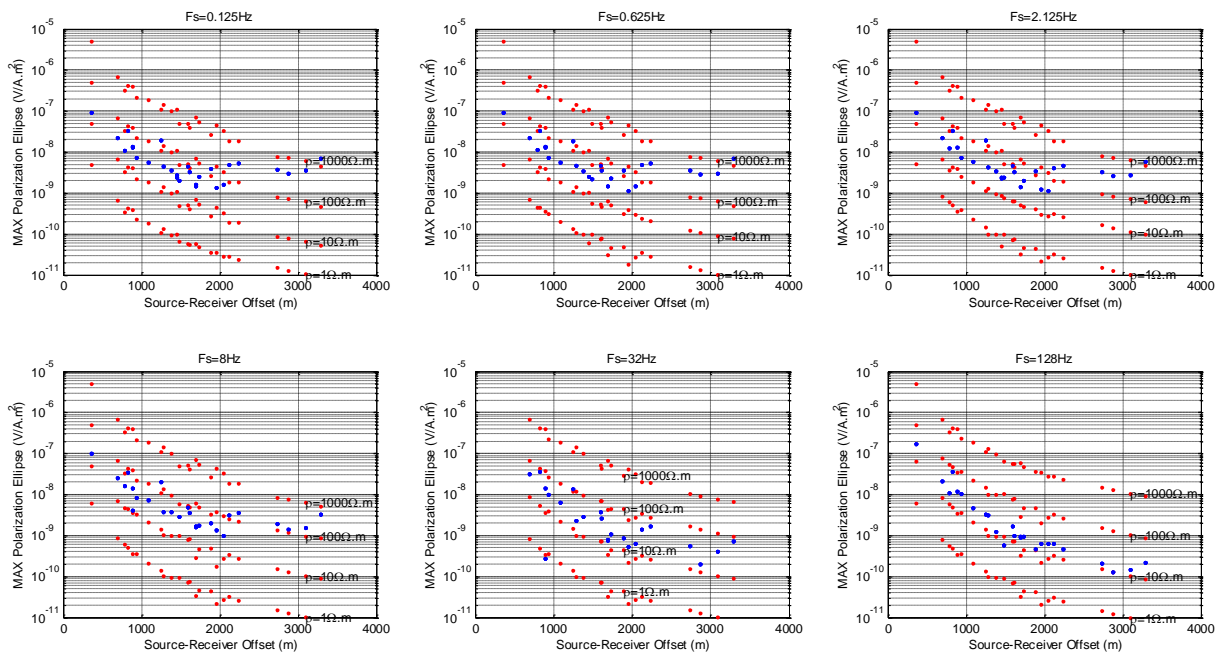
Figure 31 : Measured (blue dots) and modelled (red dots) maximum axis of the polarization ellipse of the electric field at 0.125, 0.625, 2.125, 8, 32 and 128Hz for polarization 1. Every modelled curve corresponds to a different half-space resistivity model (1, 10, 100 and 1000 Ω.m).
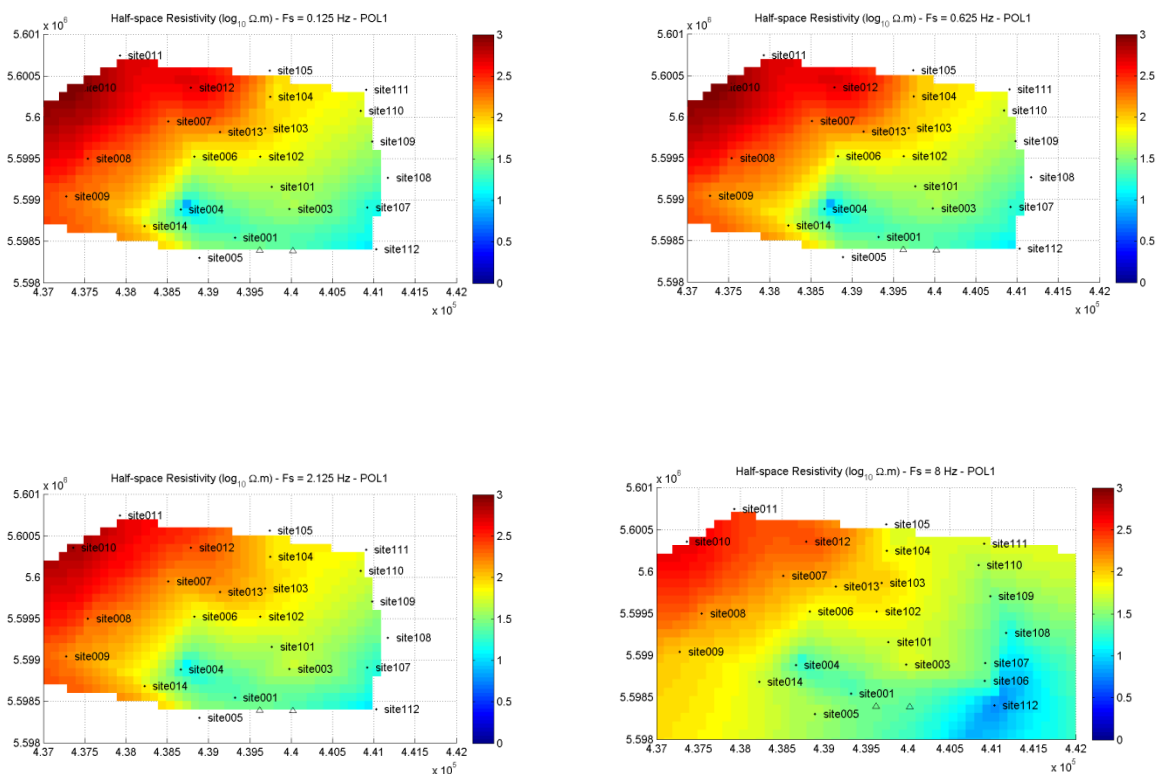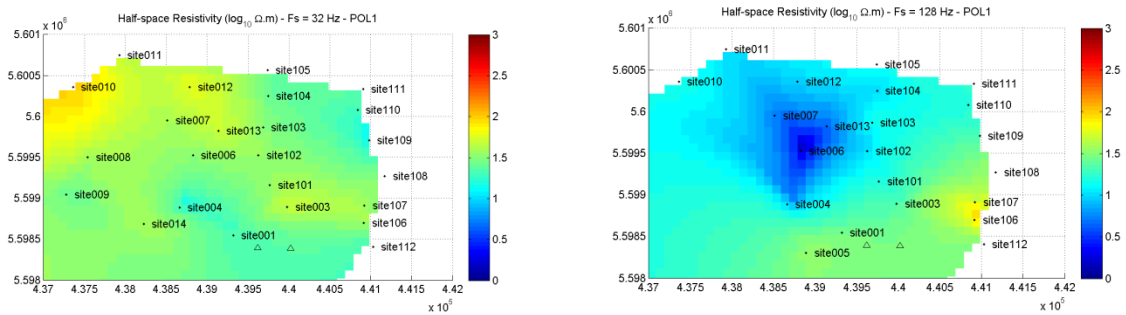
Figure 32 : Map view of the equivalent half-space resistivities (log10 Ohm.m) obtained after matching the observed maximum axis of the polarization ellipse of the electric field at 0.125, 0.625, 2.125, 8, 32 and 128Hz for polarization 1 (top left to bottom right). Coordinaates are in UTM zone 33N.
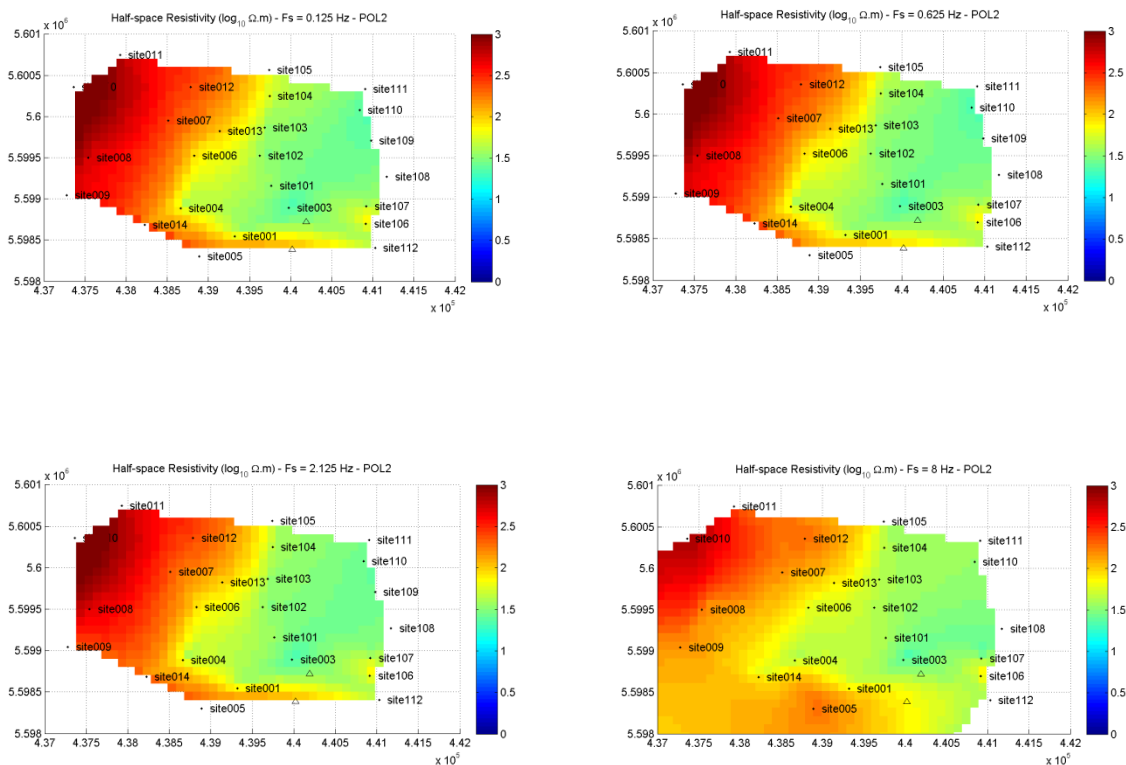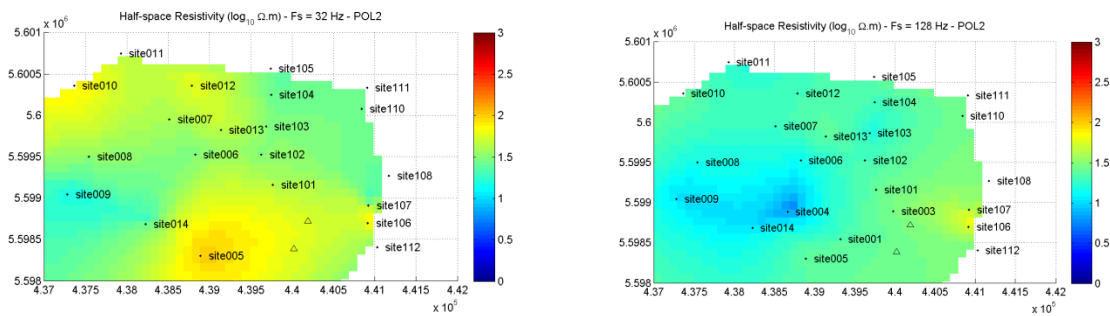
**Figure 33 : Map view of the equivalent half-space resistivities (log10 Ohm.m) obtained after matching the observed maximum axis of the polarization ellipse of the electric field at 0.125, 0.625, 2.125, 8, 32 and 128Hz for polarization 2 (top left to bottom right). Coordinaates are in UTM zone 33N.**
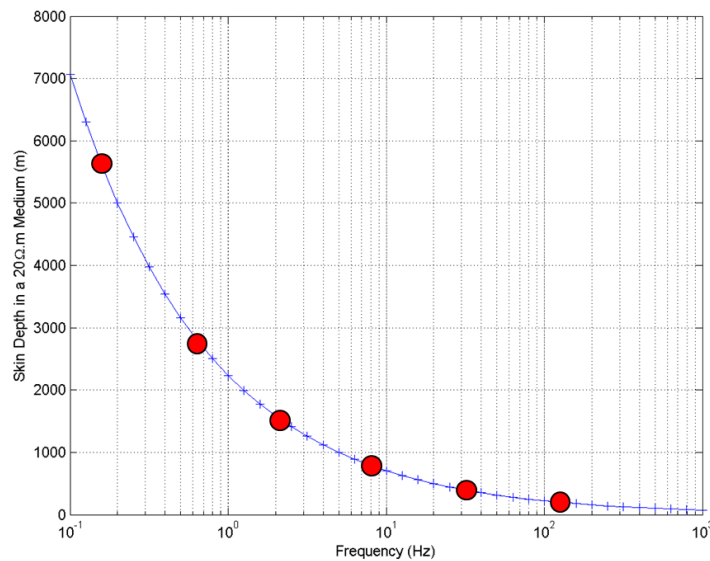
Figure 34 : Skin depth as a function of frequency for a 20 Ω.m medium.

3.4.2.3 1D inversion results & Interpretation

To convert the equivalent half-space resistivities measured at different frequencies into a resistivity depth profile, we used the smooth 1D inversion code designed by Constable et al. (1987) and Key (2009) called OCCAM1DCSEM.

Occam's inversion seeks to minimize the following unconstrained regularized functional:

$$U = \|\partial\mathbf{m}\|^2 + \|\mathbf{P}(\mathbf{m} - \mathbf{m}_*)\|^2 + \mu^{-1}\left[\|\mathbf{W}(\mathbf{d} - F(\mathbf{m}))\|^2 - \chi_*^2\right]$$

The first term is a norm of the model roughness and is computed by applying a differencing operator ∂ to the elements of the model vector **m**. For the one dimensional models considered here, m is a vector of $\log_{10}\rho$ for each layer and ∂ is chosen to be a matrix of first-differencing operators so that ∂m approximates the vertical derivative of $\log_{10}\rho$. The second term is a measure of the difference of **m** from an a priori preference model **m***. The diagonal matrix P contains scaling parameters that determine the relative weighting between the preference and the model roughness.

The roughness and preference terms in the above equation are regularizers that serve to stabilize the inversion and keep it from producing wildly oscillating resistivity structure. Finally, the third term is a measure of the misfit of the model's forward response **F(m)** (i.e., the electric and magnetic fields for model **m**) to the data **d**. **W** is a data covariance weighting function and is here selected to be a diagonal matrix with elements corresponding to inverse data standard errors. In other words, **W** weights the relative contribution of each datum to the misfit based on its uncertainty. χ_*^2 is the target misfit and its inclusion illustrates that minimizing **U** do does not necessarily find the best fitting model, but rather a smooth model that is within the specified target misfit (usually chosen to be unity). The Lagrange multiplier **μ** serves to balance the trade-off between the data fit and the model roughness and model preference. The nonlinear minimization of equation is described in Constable et al. (1987) and one of the main innovations of the Occam method is the automatic selection of **μ**.

Figure 35shows the 1D resistivity profile obtained from the smooth inversion of the CSEM data at 0.125, 0.625, 2.125, 8, 32 and 128Hz from stations 003, 101, 102, 103, 104 and 105, i.e. a north-south profile from the source. The fit between the modelled and observed data is good, demonstrating that the inversion has converged (Figure 36). We only inverted the maximum axis of the polarization ellipses of the electric field, as phases turned out to be noisier than amplitudes. Given the shallow depth of penetration of the injected current, the LEMAM source has been simplified into a horizontal electric dipole. The inverted resistivity profile shows a shallow conductive layer (<50 Ω.m) up to ~200m depth followed by a more resistive layer of around 100 Ω.m up to 1000m. At depth greater than 1000m, a very resistive body (> 1000 Ω.m) can be found. From the smooth inversion of CSEM data only, it is however difficult to establish at which depth the interfaces between the different bodies are. The smooth inversion of synthetic data generated with the same geometry and frequency as the actual profile illustrates nicely this uncertainty: the resistivity model with sharp resistivity contrasts is inverted as a smooth model with a steady increase of resistivity with depth. A-priori knowledge of the depth of the different interfaces/resistivity contrasts (e.g. from seismic data) would be required to sharpen the resistivity profile.

From the geological knowledge of the area, previous geophysical investigations (Geomedia report) and the geothermal exploration well (Figure 38), it is likely that the first few hundreds of meters conductive body observed on the inverted CSEM profile corresponds to the Quaternary and Cretaceous sediments (30-100 Ω.m). Beneath this layer, the resistivity increases as older and tighter Permo-Carbonifereous sediments can be found (resistivity ~100 Ω.m). At around 1000m depth, the resistivity increase up to a few thousands Ω.m is likely to correspond to the Proteorozoic basement.

On the other hand, we performed a 1D inversion for site 11 only located on the more resistive area from the modelling analysis (Figure 39). Similarly to the previous profile, we find a shallow conductive layer of around 20-30 Ω.m corresponding most likely to the recent sediments. However, the transition into the resistive basement is a lot sharper than along the profile suggesting that the Cretaceous/Permo-Carboniferous sediment layer is a lot thinner (<1000m). This is confirmed by the borehole Ub7, which is located on the fault block a few kilometers to the North (Figure 1). Here, the basement is found at 500m and no Permo-Carboniferous sediment has been observed (Capova, 2013).
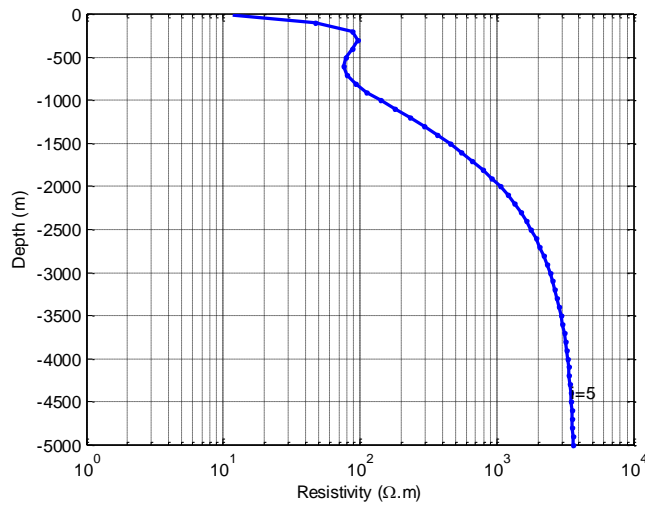
Figure 35 : 1-D resistivity profile obtained from the smooth inversion of the CSEM data at 0.125, 0.625, 2.125, 8, 32 and 128Hz from stations 003, 101, 102, 103, 104 and 105.
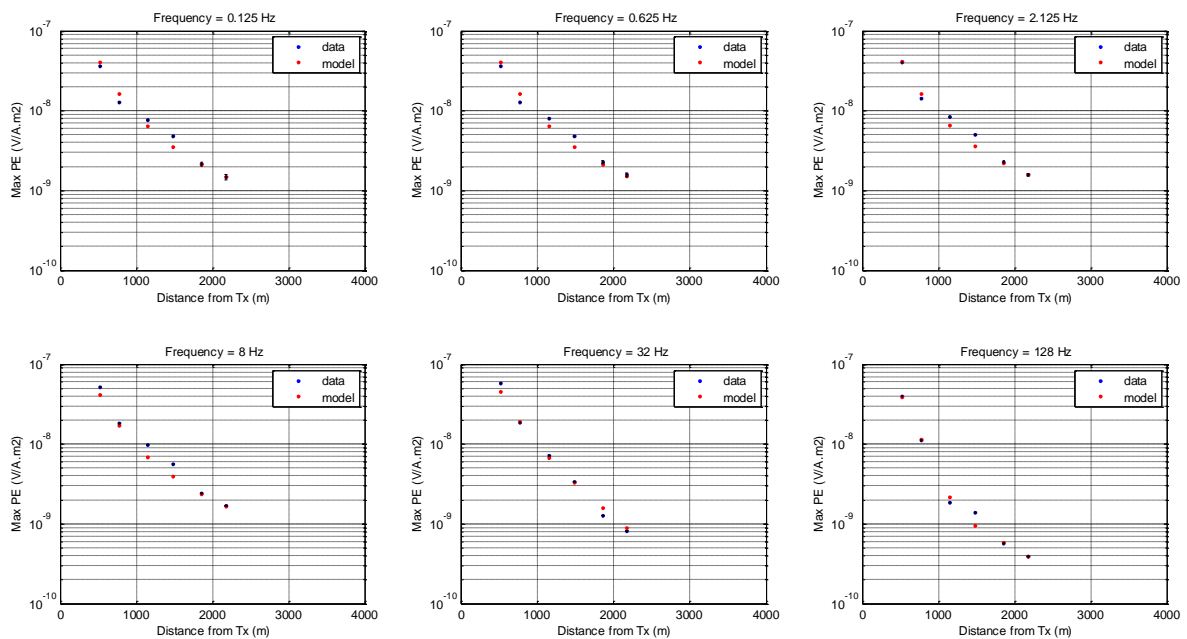

Figure 36 : 1-D resistivity profile obtained from the smooth inversion of the CSEM data at 0.125, 0.625, 2.125, 8, 32 and 128Hz from stations 003, 101, 102, 103, 104 and 105.
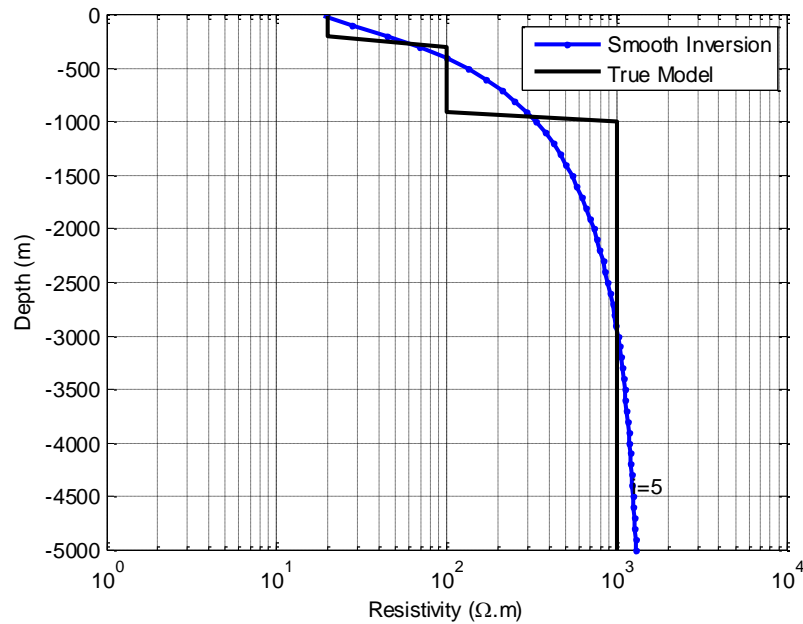
Figure 37 : Smooth inversion of synthetic data generated with the same geometry and frequency as the actual profile. The resistivity model with sharp resistivity contrasts (black) is inverted as a smooth model with a steady increase of resistivity with depth (blue).
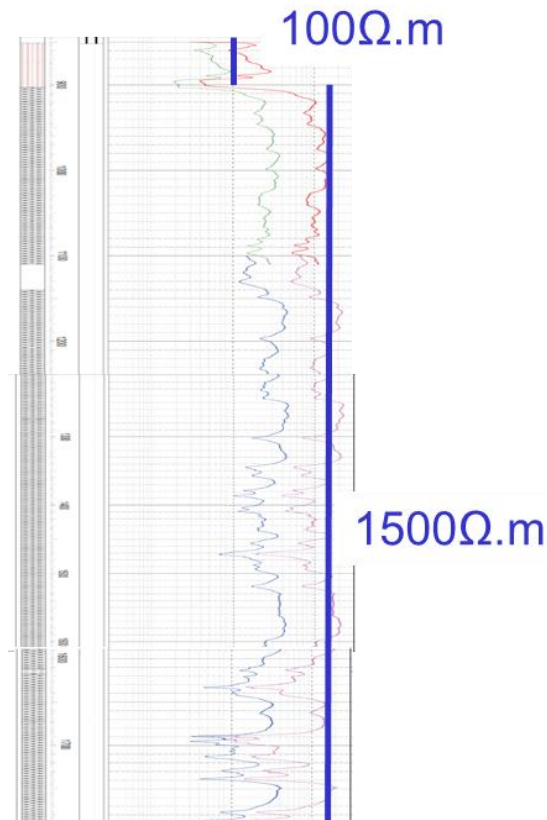
Figure 38 : Resistivity profile logged in the geothermal exploration well PVGT LT-1. Resistivity of Permo-Carbonifereous sediments is around 100 Ω.m while the Proterozoic basement exhibit resistivities greater than 1000 Ω.m.
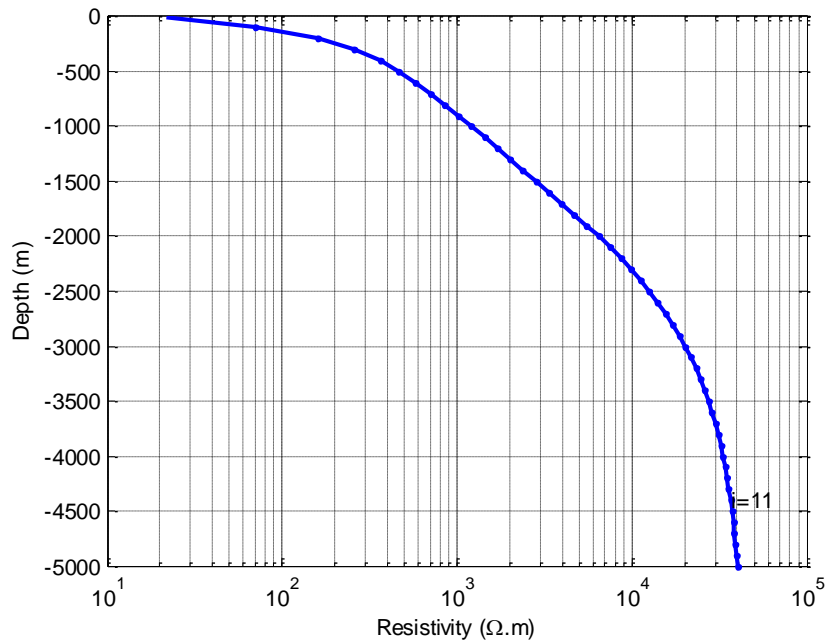
Figure 39 : 1-D resistivity profile obtained from the smooth inversion of the CSEM data at 2.125, 8 and 128Hz from station 011.

4   Conclusions & Way Forward

The objectives of the study were to

1) Improve the signal quality of MT data acquired in peri-urban areas like Litomerice area by applying robust MT signal processing using synchronous recordings performed locally and at far remote stations.
2) Successfully acquire an active Controlled Source (CSEM) survey in the Litomerice area to complement the MT dataset and demonstrate that we can retrieve realistic resistivity measurements from CSEM measurements up to the depth of the geothermal reservoirs of interest.

The first objective has been partly met as despite the use of a remote reference, MT data are still corrupted at low frequency (<5Hz) by a permanent anthropic noise source. However, at higher frequencies, reliable resistivity measurements have been obtained.

The second objective has been met as the Long Electrode Mise-à-la-Masse (LEMAM) CSEM setup has allowed acquiring good quality EM data with a minimal imprint of industrial noise and capable of imaging resistivity variations at a few kilometers depth i.e. at the depth of the geothermal reservoir of interest.

As a way forward in the next Work Package (WP8.2 application of exploration techniques) and as soon as the level of noise of an EM survey is believed to be an issue (e.g. due to the proximity of a city, train, high power line, and so on…), we strongly recommend to compliment passive MT measurements with active CSEM measurements to image resistivity variations at reservoir depth. This can be done with single or double LEMAM setups but also with conventional surface only setups – a feasibility study is required to define on a case by case basis the appropriate approach.

5   Bibliography

Bourgeois B. and Girard J. F. (2010) – First modelling results of the EM response of a CO2 storage in the Paris Basin. *Oil & Gas Science and Technology–Revue de l'Institut Français du Pétrole*, *65*(4), 597-614.

Capova Lucie, 2013, Specification of the geothermic model in the environs of several selected boreholes, Master Thesis, CHARLES UNIVERSITY, FACULTY OF SCIENCES.

Constable, S. C., R. L. Parker, and C. G. Constable, 1987, Occam's inversion — A practical algorithm for generating smooth models from electromagnetic sounding data: Geophysics, 52, 289–300.

Gamble, T., Goubau, W. M., & Clarke, J. (1979). Magnetotellurics with a remote magnetic reference. *Geophysics*, *44*(1), 53-68.

Geomedia (2006). Geophysical survey in the Litomerice surrounding. Survey report

Kong, F.N., Roth F., Olsen P.A. and Stalheim, S.O. (2009), Casing effects in the sea-to-borehole electromagnetic method, *Geophysics*, VOL. 74, NO. 5 SEPTEMBER-OCTOBER 2009; P. F77–F87, 10.1190/1.3173807

Kerry Key, 2009, 1D inversion of multicomponent, multifrequency marine CSEM data: Methodology and synthetic studies for resolving thin resistive layers, GEOPHYSICS,VOL. 74, NO. 2 !MARCH-APRIL 2009"; P. F9–F20, 12 FIGS. 10.1190/1.3058434

Chave, A. D., & Jones, A. G. (2012). *The magnetotelluric method: Theory and practice.* Cambridge University Press.

Vozoff, K. (1972). The magnetotelluric method in the exploration of sedimentary basins. *Geophysics*, *37*(1), 98-141.

Zelwer, R., & Morrison, H. F. (1972). Spatial characteristics of midlatitude geomagnetic micropulsations. *Journal of Geophysical Research*, *77*(4), 674-694.